COMMUN. MATH. SCI.
Vol. 16, No. 8, pp. 2167–2198


# NUMERICAL COMPUTATION FOR THE NON CUTOFF RADIALLY SYMMETRIC HOMOGENEOUS BOLTZMANN EQUATION*

LÉO GLANGETAS† AND IBRAHIM JRAD‡

**Abstract.** For the non cutoff radially symmetric homogeneous Boltzmann equation with Maxwellian molecules, we give the numerical solutions using symbolic manipulations and spectral decomposition of Hermite functions. The initial data can belong to some measure space.

**Keywords.** Boltzmann equation; kinetic equations; spectral decomposition; symbolic computation; numerical computation.

**AMS subject classifications.** 34K08; 35Q20; 35-04; 35P05; 35P30; 65M70.

## 1. Introduction

**1.1. The Boltzmann equation.** The Boltzmann equation, derived by Boltzmann in 1872 (and Maxwell 1866), models the behavior of a dilute gas (see [8]). As we know, Boltzmann has created a theory which described the movement of gases as balls which could bump and rebound against each other [11, 20]. This model can be considered as one of many cases which represent the so-called kinetic equation. Presently, a diverse field of sciences and applications use these models such as rarefied gas dynamics, semiconductor modeling, radiative transfer, and biological and social sciences. This type of equation is made by including a combination of a linear transport term and several interaction terms which provide the time evolution of the distribution of particles in the phase space. The equation that bears his name is the following

$$\begin{cases} \partial_t f + v.\nabla_x f = \mathbf{Q}(f,f), \\ f(t=0,x,v) = F(x,v) \end{cases}$$

with $f = f(t,x,v) \geq 0$ is the probability density to find a particle at the time $t$, on the position $x$ and with velocity $v$, where the physical and the velocity spaces are located in three dimensions. The term $v.\nabla_x f$ describes the free action of particles and $\mathbf{Q}(f,f)$ is a bi-linear operator which describes the binary collision process. It is called the Boltzmann collision operator and is given by

$$\mathbf{Q}(g,f)(v) = \int_{\mathbb{R}^3}\int_{\mathbb{S}^2} B(v-v_*,\sigma)(g'_* f' - g_* f)dv_* d\sigma$$

where we use the notation $f'_* = f(t,x,v'_*)$, $f' = f(t,x,v')$, $f_* = f(t,x,v_*)$. The symbols $v'_*$ and $v'$ are abbreviations for the expressions

$$v' = \frac{v+v_*}{2} + \frac{|v-v_*|}{2}\sigma, \;\; v'_* = \frac{v+v_*}{2} - \frac{|v-v_*|}{2}\sigma$$

where $\sigma \in \mathbb{S}^2$ and they are obtained in such a way that collision preserves momentum and kinetic energy, namely

$$v'_* + v' = v + v_*, \;\; |v'_*|^2 + |v'|^2 = |v|^2 + |v_*|^2$$

*Received: July 7, 2017; Accepted (in revised form): August 13, 2018. Communicated by Shi Jin.

†Laboratoire de Mathématiques Raphaël Salem, Université de Rouen Normandie, UMR 6085-CNRS, Avenue de l'Université, BP.12, 76801 Saint Etienne du Rouvray, France (leo.glangetas@univ-rouen.fr).

‡Supported by a grant from Lebanon, Laboratoire de Mathématiques Raphaël Salem, Université de Rouen Normandie, UMR 6085-CNRS, Avenue de l'Université, BP.12, 76801 Saint Etienne du Rouvray, France (brahimjrad92@hotmail.com).

where $|\cdot|$ is the Euclidean norm on $\mathbb{R}^3$. Note that $v$, $v_*$ are the velocities before collision and $v'$, $v'_*$ are the velocities after collision.

The non-negative cross section $B(z,\sigma)$ with $z=(v-v_*)$ depends only on $|z|$ and the scalar product $\frac{z}{|z|}\cdot\sigma=\cos\theta$ where $\theta$ is the deviation angle. Without loss of generality, we may assume in the non cutoff case that this cross section is supported on the set $\cos\theta\geq 0$. See for instance [32] for more details on the cross section and [40] for a general collision kernel. For physical models, it usually takes the form

$$B(v-v_*,\sigma)=\Phi(|v-v_*|)b(\cos\theta),\quad \cos\theta=\frac{v-v_*}{|v-v_*|}\cdot\sigma,\quad 0\leq\theta\leq\frac{\pi}{2}$$

where $\Phi(|v-v_*|)=|v-v_*|^\gamma$ is a kinetic factor and $\gamma>-3$.

In this work, we consider the spatially homogeneous case, that means the density distribution $f=f(t,v)$ depends on the variables $t\geq 0$, $v\in\mathbb{R}^3$ and is uniform with respect to $x$. So that the Boltzmann equation reads as

$$\begin{cases}\partial_t f=\mathbf{Q}(f,f),\\ f(t=0,v)=F(v)\end{cases}\tag{1.1}$$

where the initial data $F$ is depends only on $v$. For the collision kernel, we study only the Maxwellian molecules, that means the kinetic factor $\Phi\equiv 1$, and both cutoff and non cutoff (see [12–15, 17, 26, 33]):

$$\bullet\ \text{cutoff case:}\quad b(\cos\theta)\equiv\frac{1}{4\pi},\tag{1.2}$$

$$\bullet\ \text{non cutoff case:}\quad b(\cos\theta)\underset{0}{\approx}\frac{1}{|\theta|^{2+2s}},\quad 0<s<1.\tag{1.3}$$

**1.2. Results on the Boltzmann equation.** With the previous assumption (the non cutoff case) on the cross-section, there is existence of a weak solution for the Boltzmann equation (1.1) for a positive initial value $F\in L^1_{2+\delta}(\mathbb{R}^3)$. See [39] and many others. Moreover, it is well-known that there is a regularization effect in Sobolev and Schwartz or analytic spaces for any time $t>0$ (we refer the reader to [12, 13] and recently [1]) and that the solutions converge to the Maxwellian distribution when the time tends to infinity [26].

An important point is that our distribution lives in a multidimensional space: this reason makes us think that we have a numerical problem because in this case the computational cost is more or less forbidden [20]. The study of the numerical part for kinetic equations is not obvious due to many difficulties arising from the computational cost. To clarify more, we mention two of these difficulties: it is clear the appearing of multiple scales, and then to get out of the resolution of the stiff dynamics, one should build suitable numerical schemes [2, 18, 19, 27–29]. The other one is that the collision operator is defined by multidimensional integrals and to compute one should solve it point by point as physical space [22, 37]. To treat kinetic equations numerically, there are several ways which are used over the centuries until now: probabilistic numerical methods such as Direct Simulation Monte Carlo (DSMC) schemes [3, 11], and, deterministic numerical methods such as finite volume, semi-Lagrangian and spectral schemes [20].

There are two important deterministic methods which are used in the past decades: the discrete velocity method (DVM) [6, 9, 10, 25, 35, 38] and the Fourier spectral method (FSM) [7, 10, 23, 36, 37]. Due to its discrete nature, the DVM preserves positivity of the distribution function, the H-theorem and the exact conservation of mass, energy and

momentum. Note that the Fourier spectral method is based on two main things: the truncation of the collision operator and the restriction of the distribution function to an appropriate cube, for more details see [34, 37].

Our goal is to present an alternative method to solve formally and numerically the homogeneous Boltzmann equation in the non cutoff case. In this work, we consider the radial symmetric case and we use a spectral method: we first compute the spectral coefficients of the solution with a formal computation software (Maple®13 and 2016; most of the codes are provided in Appendix E). We then approximate these exact solutions and check the numerical results.

The used method helps us to motivate our work in several ways. In the physical view, it lets us understand more about the behavior of the solutions, see for example the measure-type initial data. In the numerical view, exact spectral solutions are constructed that could be used to test numerical algorithms that are similar to the exact formulas for higher order moments defined in the paper of Krook-Wu [30] by equation (35). On the other hand, we study the accuracy (using the BKW solution) and duration of this symbolic method. Recall that the explicit BKW solution (3.4) obtained independently in [4, 30] is used to test the accuracy of the numerical methods in the case of a regular collision kernel $B \equiv \frac{1}{4\pi}$, see for example [10, 23]. Finally, we do hope that our work will give some clues to formulate new mathematical conjectures.

The paper is organized as follows. In Section 2, we state the main theoretical results. The numerical details are provided in Section 3. Sections 4 and 5 present the numerical results of the Boltzmann equation with different initial data for the Cauchy problem: we estimate in Section 4 the error between the approximate spectral solution and the explicit BKW solution. In Section 5, we consider the case of a measure initial data. After that, we give a conclusion for this work in Section 6. The paper ends with an appendix where we set some technical results and we provide some algorithms.

## 2. Theoretical results

In this section, we present some theoretical parts: we begin by linearizing the Boltzmann equation and giving the spectral decomposition of this equation.

**2.1. Linearization of the Boltzmann equation.** We remark that $Q(\mu,\mu)=0$ where the Maxwellian distribution is defined by

$$\mu(v)=\frac{1}{(2\pi)^{3/2}}e^{-\frac{|v|^2}{2}}$$

and it is a stationary solution of the Boltzmann equation. We consider now a perturbation $g$ of the Maxwellian distribution. Then the solution $f$ of (1.1) can be written as

$$f(t,v)=\mu(v)+\sqrt{\mu(v)}g(t,v),$$
$$F(v)=\mu(v)+\sqrt{\mu(v)}G(v).$$

It is easy to show that $g$ is a solution of the Cauchy problem

$$\begin{cases}\partial_t g+\mathcal{L}(g)=\mathbf{\Gamma}(g,g),\\ g|_{t=0}=g(0,v)=G(v)\end{cases}\tag{2.1}$$

where

$$\mathcal{L}(g)=-\frac{1}{\sqrt{\mu}}[\mathbf{Q}(\sqrt{\mu}g,\mu)+\mathbf{Q}(\mu,\sqrt{\mu}g)]$$

is a linear operator and

$$\mathbf{\Gamma}(g,h)=\frac{1}{\sqrt{\mu}}\mathbf{Q}(\sqrt{\mu}g,\sqrt{\mu}h)$$

is a nonlinear operator. We decompose the solution of (2.1) into a linear and nonlinear part:

$$g(t,v)=\underbrace{e^{-t\mathcal{L}}G(v)}_{\text{linear part}}+\underbrace{e^{-t\mathcal{L}}h(t,v)}_{\text{nonlinear part}}$$

where $e^{\alpha\mathcal{L}}$ is the exponential of the linear operator defined by its spectral decomposition (see below) and the new function $h(t,v)$ satisfies the following equation

$$\begin{cases}\partial_t h=e^{t\mathcal{L}}\mathbf{\Gamma}(e^{-t\mathcal{L}}(G+h),e^{-t\mathcal{L}}(G+h)),\\ h(0,v)=0.\end{cases}\tag{2.2}$$

The linearized operator $\mathcal{L}$ is a positive unbounded symmetric operator on $L^2(\mathbb{R}^3_v)$ (see [11,31–33]) with the kernel

$$\mathcal{N}=\text{span}\left\{\sqrt{\mu},\sqrt{\mu}v_1,\sqrt{\mu}v_2,\sqrt{\mu}v_3,\sqrt{\mu}|v|^2\right\}.$$

From a rescaling argument (see Appendix B), we can always assume that the initial condition $G$ satisfies

$$G\in\mathcal{N}^{\perp}.$$

In [32], for the radially symmetric case, the authors show that the linear Boltzmann operator behaves like the fractional harmonic oscillator $\mathcal{H}^s$ $(0<s<1)$ with

$$\mathcal{H}=-\Delta+\frac{|v|^2}{4}.$$

We study in the next section the spectral properties of the operators $\mathcal{L}$ and $\mathbf{\Gamma}$.

**2.2. The spectral problem.** We introduce now an orthonormal basis of $L^2_r(\mathbb{R}^3)$, the radial symmetric functions of $L^2(\mathbb{R}^3)$ involving the generalized Laguerre polynomials $L_n^{\ell+\frac{1}{2}}$: for that, we set for any $n\geq 0$

$$\varphi_n(v)=\left(\frac{n!}{\sqrt{2}\Gamma(n+3/2)}\right)^{1/2}e^{-\frac{|v|^2}{4}}L_n^{[\frac{1}{2}]}\left(\frac{|v|^2}{2}\right)\frac{1}{\sqrt{4\pi}}\tag{2.3}$$

where $\Gamma(\cdot)$ is the standard gamma function, for all $x>0$

$$\Gamma(x)=\int_0^{+\infty}t^{x-1}e^{-t}dt$$

and the Laguerre polynomial $L_n^{[\alpha]}$ of order $\alpha$, degree $n$ is

$$L_n^{[\alpha]}(x)=\sum_{r=0}^{n}(-1)^{n-r}\frac{\Gamma(\alpha+n+1)}{r!(n-r)!\Gamma(\alpha+n-r+1)}x^{n-r}.$$

We have the spectral decomposition for the linear Boltzmann operator

$$\mathcal{L}\varphi_n = \lambda_n \varphi_n$$

for all $n \geq 0$ with $\varphi_0 = \sqrt{\mu}$, $\lambda_0 = 0$ and for $n \geq 1$

$$\lambda_n = \int_0^\pi 2\pi \sin\theta b(\cos\theta) \left\{1 - \cos^{2n}\left(\frac{\theta}{2}\right) - \sin^{2n}\left(\frac{\theta}{2}\right)\right\} d\theta \tag{2.4}$$

where $b(\cos(\theta))$ is defined from the collision kernel (see (1.2)-(1.3)). The two families $(\varphi_n)_{n\geq 0}$ and $(\lambda_n)_{n\geq 0}$ represent the eigenvectors and the eigenvalues of $\mathcal{L}$. Remark that this diagonalization of the linearized Boltzmann operator with Maxwellian molecules is also verified in the cutoff case (see [5, 11, 21, 31, 32]).

We consider the spectral expansion

$$g(t,v) = \sum_{n=0}^{\infty} g_n(t)\varphi_n(v), \quad G(v) = \sum_{n=0}^{\infty} G_n \varphi_n(v) \tag{2.5}$$

where $g_n(t) = \Big(g(t,\cdot), \varphi_n(\cdot)\Big)_{L^2}$ and $G_n = \Big(G, \varphi_n\Big)_{L^2}$. By definition, we have

$$e^{-t\mathcal{L}}G(v) = \sum_{n=0}^{\infty} e^{-\lambda_n t} G_n \varphi_n(v).$$

It is the solution of the equation

$$\begin{cases} \partial_t g^{lin} + \mathcal{L} g^{lin} = 0, \\ g^{lin}(0,v) = G(v). \end{cases}$$

Then the operator $\mathbf{\Gamma}$ satisfies for $p, q \geq 0$

$$\mathbf{\Gamma}(\varphi_p, \varphi_q) = \mu_{pq}\varphi_{p+q}$$

where the nonlinear eigenvalues are given by

$$\begin{cases} \mu_{pq} = \left(\dfrac{(2p+2q+1)!}{(2p+1)!(2q+1)!}\right)^{\frac{1}{2}} \displaystyle\int_0^\pi 2\pi \sin\theta b(\cos\theta) \left\{\sin^{2p}\left(\frac{\theta}{2}\right)\cos^{2q}\left(\frac{\theta}{2}\right)\right\} d\theta \quad \text{for } p \geq 1, \\ \mu_{0q} = -\displaystyle\int_0^\pi 2\pi \sin\theta b(\cos\theta) \left\{1 - \cos^{2q}\left(\frac{\theta}{2}\right)\right\} d\theta. \end{cases} \tag{2.6}$$

We note that $\lambda_n = -(\mu_{0n} + \mu_{n0})$. Following [33], we therefore derive from (2.1) the following infinite system of ordinary differential equations:

$$\begin{cases} g_0'(t) = 0, \quad g_1'(t) = 0 \quad \text{and for all} \quad n \geq 2 \\ g_n'(t) + \lambda_n g_n(t) = \displaystyle\sum_{\substack{p+q=n \\ 0\leq p,q\leq n}} \mu_{pq} g_p(t) g_q(t) \end{cases} \tag{2.7}$$

with $\lambda_1 = 0$, $\mu_{00} = 0$, $\mu_{10} = -\mu_{01}$ and the initial conditions (see (2.5))

$$g_n(0) = G_n \quad \text{for} \quad n \geq 0.$$

The goal is to study the behavior of each function $g_n$.

In the rest, we will focus on the computation and properties of the intermediate solution $h(t,v)$.

PROPOSITION 2.1. *We assume that $G\in\mathcal{N}^{\perp}$. Then the intermediate solution $h(t,v)$ defined by (2.2) satisfies*

$$h(t,v)=\sum_{n=0}^{\infty}h_n(t)\,\varphi_n(v)$$

*where $h_0\equiv h_1\equiv h_2\equiv h_3\equiv 0$ and for all $n\geq 4$*

$$h_n(t)=\sum_{\substack{p+q=n\\ 2\leq p,q\leq n-2}}\int_0^t \mu_{pq}\,e^{-(\lambda_p+\lambda_q-\lambda_n)s}\left(G_p+h_p(s)\right)\left(G_q+h_q(s)\right)ds. \tag{2.8}$$

REMARK 2.1. Since $G\in\mathcal{N}^{\perp}$, we have $g(t,\cdot)\in\mathcal{N}^{\perp}$ for all $t>0$. As we have seen before, we divide the function $g$ in two parts as follows:

$$g(t,v)=\underbrace{\sum_{n=2}^{\infty}e^{-\lambda_n t}G_n\,\varphi_n(v)}_{g^{lin}(t,v)}+\underbrace{\sum_{n=2}^{\infty}e^{-\lambda_n t}h_n(t)\,\varphi_n(v)}_{g^{n\ell}(t,v)} \tag{2.9}$$

therefore the formal solution $f(t,v)$ can be written as

$$f(t,v)=\mu(v)+\sqrt{\mu(v)}\sum_{n=2}^{\infty}\left(e^{-\lambda_n t}G_n+e^{-\lambda_n t}h_n(t)\right)\varphi_n(v).$$

*Proof.* (Proof of Proposition 2.1.) As $G\in\mathcal{N}^{\perp}$, we get $G_0=G_1=0$ and we can verify from (2.7) that

$$g_0(t)=g_1(t)=0,\ g_2(t)=G_2\,e^{-\lambda_2 t},\ g_3(t)=G_3\,e^{-\lambda_3 t}$$

and therefore $h_0\equiv h_1\equiv h_2\equiv h_3\equiv 0$. By (2.7), we may write

$$g_n(t)=e^{-\lambda_n t}G_n+e^{-\lambda_n t}h_n(t) \tag{2.10}$$

and

$$g_n'(t)+\lambda_n g_n(t)=\sum_{\substack{p+q=n\\ 2\leq p,q\leq n-2}}\mu_{pq}\,g_p(t)\,g_q(t). \tag{2.11}$$

We plug again the value of $g_n$ from (2.10) into the equation (2.11) and we get

$$h_n'(t)=e^{\lambda_n t}\sum_{\substack{p+q=n\\ 2\leq p,q\leq n-2}}\mu_{pq}\,g_p(t)\,g_q(t).$$

Note that $h_n(0)=g_n^{n\ell}(0)=0$. Finally, plugging the expression of $g_p$ and $g_q$ from (2.10) into the previous equation and integrating, we prove (2.8). Concerning the exact expression of the eigenvalue $\lambda_n$ and $\mu_{pq}$, see [33]. This concludes the proof. ∎

We now introduce the following notations. For a $k$-uplet $\alpha \in \mathbb{N}^k$,

$$\Lambda_\alpha = \lambda_{\alpha_1} + \lambda_{\alpha_2} + \cdots + \lambda_{\alpha_k},$$
$$G^\alpha = G_{\alpha_1} \times G_{\alpha_2} \cdots \times G_{\alpha_k}.$$

PROPOSITION 2.2. *For each integer $n \geq 4$, we define $I_n$ a set of admissible indices*

$$I_n = \left\{ \alpha \in \mathbb{N}^k \,\middle|\, k \in \mathbb{N}^*,\ \alpha_i \geq 2,\ |\alpha| = n \right\}.$$

*Then for each multi-index $\alpha, \beta, \in I_n$ there exist some real coefficients $c_\beta^\alpha$ which depend only on $\lambda_2, \ldots, \lambda_n$ and $\mu_{pq}$ for $2 \leq p, q \leq n-2$, $p+q \leq n$ such that*

$$h_n(t) = \sum_{\alpha,\beta \in I_n} c_\beta^\alpha G^\alpha \left(1 - e^{-(\Lambda_\beta - \lambda_n)t}\right). \tag{2.12}$$

*Proof.* We compute directly from (2.8)

$$h_4(t) = c_{(2,2)}^{(2,2)} {G_2}^2 \left(1 - e^{-(\Lambda_{(2,2)} - \lambda_4)t}\right)$$

where

$$c_{(2,2)}^{(2,2)} = \frac{\mu_{22}}{(\Lambda_{(2,2)} - \lambda_4)}$$

and

$$h_5(t) = c_{(2,3)}^{(2,3)} G_2 G_3 \left(1 - e^{-(\Lambda_{(2,3)} - \lambda_5)t}\right) + c_{(3,2)}^{(3,2)} G_3 G_2 \left(1 - e^{-(\Lambda_{(3,2)} - \lambda_5)t}\right)$$

where

$$c_{(2,3)}^{(2,3)} = \frac{\mu_{23}}{(\Lambda_{(2,3)} - \lambda_5)} \quad \text{and} \quad c_{(3,2)}^{(3,2)} = \frac{\mu_{32}}{(\Lambda_{(3,2)} - \lambda_5)}.$$

We prove the result by induction. Then we can suppose that (2.12) is true for each $h_{n'}$ $(4 \leq n' \leq n-1)$. We will use the integral expression (2.8) of $h_n$. We consider two integers $p, q$ such that $2 \leq p, q \leq n-2$ and $p+q = n$. Then from (2.12)

$$h_p(t) = \sum_{\alpha,\beta \in I_p} c_\beta^\alpha G^\alpha \left(1 - e^{-(\Lambda_\beta - \lambda_p)t}\right),$$
$$h_q(t) = \sum_{\alpha',\beta' \in I_q} c_{\beta'}^{\alpha'} G^{\alpha'} \left(1 - e^{-(\Lambda_{\beta'} - \lambda_q)t}\right).$$

From the integral formula (2.8) we get

$$h_n(t) = \int_0^t \sum_{\substack{p+q=n \\ 2 \leq p,q \leq n-2}} (A + B + C + D)\, ds$$

with

$$A = \mu_{pq} G_p G_q e^{-(\lambda_p + \lambda_q - \lambda_n)s},$$
$$B = \sum_{\alpha',\beta' \in I_q} \mu_{pq} c_{\beta'}^{\alpha'} G_p G^{\alpha'} \left(e^{-(\lambda_p + \lambda_q - \lambda_n)s} - e^{-(\lambda_p + \Lambda_{\beta'} - \lambda_n)s}\right),$$

$$C=\sum_{\alpha,\beta\in I_p}\mu_{pq}\,c_\beta^\alpha\,G^\alpha\,G_q\,(e^{-(\lambda_p+\lambda_q-\lambda_n)\,s}-e^{-(\Lambda_\beta+\lambda_q-\lambda_n)\,s}),$$

$$D=\sum_{\alpha,\beta\in I_p}\sum_{\alpha',\beta'\in I_q}\mu_{pq}\,c_\beta^\alpha\,c_{\beta'}^{\alpha'}\,G^\alpha\,G^{\alpha'}\quad\times$$

$$(e^{-(\lambda_p+\lambda_q-\lambda_n)\,s}-e^{-(\Lambda_\beta+\lambda_q-\lambda_n)\,s}-e^{-(\lambda_p+\Lambda_{\beta'}-\lambda_n)\,s}+e^{-(\Lambda_\beta+\Lambda_{\beta'}-\lambda_n)\,s}).$$

Expanding each of the previous terms and integrating over $[0,t]$, we get the result (2.12) since each number $\lambda_p+\lambda_q-\lambda_n$, $\Lambda_\beta+\lambda_q-\lambda_n$, $\lambda_p+\Lambda_{\beta'}-\lambda_n$, $\Lambda_\beta+\Lambda_{\beta'}-\lambda_n$ is positive from the next lemma and $|\alpha|=|\beta|=p$, $|\alpha'|=|\beta'|=q$ and $p+q=n$. ∎

LEMMA 2.1. *The linear eigenvalues $\lambda_n$ defined in (2.4) for the radially symmetric spatially homogeneous Boltzmann equation verify the following property*

$$\lambda_{\alpha_1+\cdots+\alpha_k}<\lambda_{\alpha_1}+\cdots+\lambda_{\alpha_k}(=\Lambda_\alpha)$$

*for multi-index $\alpha\in(\mathbb{N}\setminus\{0,1\})^k$.*

*Proof.* By [33], we may write

$$\lambda_{\alpha_1+\alpha_2}<\lambda_{\alpha_1}+\lambda_{\alpha_2}$$

then by iteration, we have

$$\lambda_{(\alpha_1+\cdots+\alpha_k)+\alpha_{k+1}}<\lambda_{\alpha_1+\cdots+\alpha_k}+\lambda_{\alpha_{k+1}}<(\lambda_{\alpha_1}+\cdots+\lambda_{\alpha_k})+\lambda_{\alpha_{k+1}}.$$

∎

## 3. Numerical computations

From the previous section, we set the following approximate spectral solution

$$\begin{cases} f_N(t,v)=\mu(v)+\sqrt{\mu(v)}\left(\displaystyle\sum_{n=0}^{N}e^{-\lambda_n t}(G_n+h_n(t))\,\varphi_n(v)\right),\\[2ex] h_n(t)=\displaystyle\sum_{\substack{p+q=n\\ 2\le p,q\le n-2}}\int_0^t\mu_{pq}\,e^{-(\lambda_p+\lambda_q-\lambda_n)s}\,\big(G_p+h_p(s)\big)\,\big(G_q+h_q(s)\big)\,ds \end{cases} \tag{3.1}$$

with the approximate initial data

$$F_N(v)=\mu(v)+\sqrt{\mu(v)}\left(\sum_{n=0}^{N}G_n\,\varphi_n(v)\right). \tag{3.2}$$

The eigenfunctions $\varphi_n(v)$ are explicitly given by the formula (2.3). The eigenvalues defined by (2.6) and (2.4) are computed by an integral which involves the collision kernel $b(\cos\theta)$. We distinguish the two cases:

(i) The cutoff case: $b(\cos\theta)\equiv\frac{1}{4\pi}$, that is

$$2\pi\sin\theta\,b(\cos\theta)=\frac{1}{2}\sin\theta,\qquad\theta\in[0,\pi]. \tag{3.3}$$

The aim of studying this case is to compare the spectral solutions with the explicit $f_{\mathrm{BKW}}$ solution [4,30] (see Remark A.1 in Appendix A).

$$f_{\mathrm{BKW}}(t,v)=\frac{1}{2(2\pi)^{\frac{3}{2}}(1-\mathrm{e}^{-t/6})^{\frac{5}{2}}}\left[(2-5\,\mathrm{e}^{-t/6})+\frac{\mathrm{e}^{-t/6}}{1-\mathrm{e}^{-t/6}}\,|v|^2\right]\mathrm{e}^{-\frac{|v|^2}{2\left(1-\mathrm{e}^{-t/6}\right)}}. \tag{3.4}$$

(ii) The non cutoff case: we recall that the collision kernel has a singularity $b(\cos\theta)\approx\theta^{-(2+2s)}$ for $\theta=0$ (see (1.3)). For sake of simplicity we consider for a given $s\in]0,1[$ the following form

$$2\pi\sin\theta b(\cos\theta)=\begin{cases}\sin^{-(1+2s)}\left(\frac{\theta}{2}\right) & \text{if} \quad \theta\in[0,\frac{\pi}{2}[,\\ 0 \quad \text{if} \quad \theta\in[\frac{\pi}{2},\pi].\end{cases} \tag{3.5}$$

In the specific case $s=\frac{1}{2}$, we get, by symbolic computations, the exact value of the eigenvalues, although for $s\neq\frac{1}{2}$, we get only approximate values.

In this section, we begin by giving the exact and approximate values of the eigenvalues and the estimates of the error. After that we present the method to compute the linear and nonlinear part of the solution and give some theoretical estimates of the error in the linear case.

**3.1. Computation of the linear eigenvalues.** The linear eigenvalue $\lambda_n$ is given by simple 1-dimensional integral (2.4).

**(i) Cutoff case.** The collision kernel $b(\cos\theta)$ is regular and the approximate value is easily computed with standard method. We use the numerical tool of Maple

$$\texttt{int(function(}\theta\texttt{),}\theta\texttt{=0..}\pi\texttt{,numeric)}\simeq\int_0^\pi \texttt{function}(\theta)\,d\theta$$

with 5, 10 or 20 significant digits. In the special case of the BKW solution, the form of the eigenvalues is explicit and given by Proposition A.3.

**(ii) Non cutoff case.** We recall that the collision kernel $b(\cos\theta)\approx\theta^{-(2+2s)}$ is singular but is controlled by the other terms $\sin\theta(1-\cos^{2n}(\theta/2)-\sin^{2n}(\theta/2))$. To avoid a "division by zero" error, we use the following form

$$\texttt{int(function(}\theta\texttt{),}\theta=10^{-40}\texttt{..}\pi\texttt{,numeric)}\simeq\int_0^\pi \texttt{function}(\theta)\,d\theta$$

to compute an approximate value $\lambda_n^{\text{appr.}}$ with the algorithm 4 of Appendix E. In the special case $s=\frac{1}{2}$ (see (3.5)), we compute with the algorithm 4-bis the symbolic value $\lambda_n^{\text{exact}}$ which is given for $n\geq 2$ by the integral

$$\lambda_n=\int_0^{\pi/2}\frac{1}{\sin^2\left(\frac{\theta}{2}\right)}\left\{1-\cos^{2n}\left(\frac{\theta}{2}\right)-\sin^{2n}\left(\frac{\theta}{2}\right)\right\}d\theta.$$

We first reduce the trigonometric fraction inside the integral by the symbolic tool of Maple:

$$\texttt{simplify}\left(\frac{1}{\sin^2\left(\frac{\theta}{2}\right)}\left(1-\cos^{2n}\left(\frac{\theta}{2}\right)-\sin^{2n}\left(\frac{\theta}{2}\right)\right)\right)$$

which removes the singularity of the collision kernel and gives a regular trigonometric polynomial. Then the symbolic integration

$$\texttt{int(function(}\theta\texttt{),}\theta=0\texttt{..}\pi\texttt{)}=\int_0^\pi \texttt{function}(\theta)\,d\theta$$

gives the exact value $\lambda_n^{\text{exact}}$. We then estimate the relative error $|\lambda_n^{\text{exact}}-\lambda_n^{\text{appr.}}|/\lambda_n^{\text{exact}}$ in the numerical Table 3.1.

| | Exact value | Approximate value | Relat. error |
|---|---|---|---|
| $\lambda_1$ | $0$ | $0$ | – |
| $\lambda_2$ | $1+\frac{1}{2}\pi$ | 2.5707963267948966193 | $2.7\times10^{-20}$ |
| $\lambda_3$ | $\frac{3}{2}+\frac{3}{4}\pi$ | 3.8561944901923449289 | $1.4\times10^{-20}$ |
| $\lambda_4$ | $\frac{23}{12}+\frac{15}{16}\pi$ | 4.8619097794070978277 | $5.3\times10^{-21}$ |
| $\lambda_{10}$ | $\frac{61717}{16128}+\frac{109395}{65536}\pi$ | 9.0707560428160875528 | $1.7\times10^{-21}$ |
| $\lambda_{20}$ | $\frac{60225247403}{9906683904}+\frac{83945001525}{34359738368}\pi$ | 13.754545239649748132 | $2.6\times10^{-20}$ |
| $\lambda_{30}$ | $\frac{382807351536613}{48879680618496}+\frac{54496920530418135}{18014398509481984}\pi$ | 17.335530084539302322 | $6.4\times10^{-21}$ |
| $\lambda_{40}$ | $\frac{965743814285544815866 67}{103659924891501173145 6}+\frac{663414737436726405380 25\pi}{188894659314785808547 84}$ | 20.350013652434449681 | $5.0\times10^{-20}$ |

TABLE 3.1. *Symbolic and numerical computation of $\lambda_n$ with 20 significant digits, non cutoff case.*

**3.2. Computation of the nonlinear eigenvalues.** The nonlinear eigenvalues $\mu_{pq}$ are also given by the 1-dimensional integral (2.6) and take an explicit form in the cutoff case $b(\cos\theta)\equiv\frac{1}{4\pi}$ (see Proposition A.3). We apply in the cutoff and non cutoff case the same numerical tool of Maple as in the previous section using algorithm 4 for a numerical computation of $\mu_{pq}^{\text{approx.}}$.

In the special case (3.5) where we take $s=\frac{1}{2}$, the symbolic value $\mu_{pq}^{\text{exact}}$ of

$$\mu_{pq}=\left(\frac{(2p+2q+1)!}{(2p+1)!(2q+1)!}\right)^{\frac{1}{2}}\int_0^{\pi/2}\frac{1}{\sin^2\left(\frac{\theta}{2}\right)}\left\{\sin^{2p}\left(\frac{\theta}{2}\right)\cos^{2q}\left(\frac{\theta}{2}\right)\right\}d\theta.$$

is computed by the algorithm 4-bis for $p+q=n=2,\dots,N=40$. After that, we present in Table (3.2) some symbolic and numerical values of results including the relative error $|\mu_{pq}^{\text{exact}}-\mu_{pq}^{\text{appr.}}|/\mu_{pq}^{\text{exact}}$. The relative error on the linear and nonlinear eigenvalues using

| | Exact value | Approximate value | Relat. error |
|---|---|---|---|
| $\mu_{1,1}$ | $\sqrt{30}\left(\frac{1}{6}+\frac{1}{12}\pi\right)$ | 2.3468052315616459661 | $5.2\times10^{-20}$ |
| $\mu_{1,2}$ | $\sqrt{7}\left(\frac{1}{2}+\frac{3}{16}\pi\right)$ | 2.8813518209196856030 | $1.1\times10^{-20}$ |
| $\mu_{2,1}$ | $\sqrt{7}\left(\frac{1}{16}\pi\right)$ | 0.51949205512913010260 | $1.3\times10^{-20}$ |
| $\mu_{1,19}$ | $\sqrt{2460}\left(\frac{4001928871}{59440103424}+\frac{1472719325}{68719476736}\pi\right)$ | 6.6786311833698659912 | $1.4\times10^{-20}$ |
| $\mu_{10,10}$ | $\sqrt{627967520180}\left(\frac{1}{69730304}+\frac{12155\pi}{4810363371 52}\right)$ | 0.074270916564345586742 | $2.8\times10^{-20}$ |
| $\mu_{19,1}$ | $\sqrt{2460}\left(\frac{-108158197}{59440103424}+\frac{39803225}{68719476736}\pi\right)$ | 0.17472370665141693658$e$−5 | $2.2\times10^{-19}$ |

TABLE 3.2. *Symbolic and numerical computation of $\mu_{pq}$ with 20 significant digits, non cutoff case.*

20 significant digits remains less than $10^{-18}$ and the computing time is less than 600 seconds (in each type of kernel) for a degree of freedom $N=40$. For large $N$, the computation time of the eigenvalues is much lower than the calculation time for the nonlinear term $h_n(t)$ (many hours for $N=40$), see Figure 4.4 on the right.

**3.3. Numerical solutions of the linear problem.** We introduce from (2.9) the approximation of the linear solution

$$g_N^{\ell in}(t,v) = \sum_{n=0}^{N} e^{-\lambda_n t} G_n \varphi_n(v) \tag{3.6}$$

where the reals $G_n$ are the given initial spectral coefficients. In order to compute the linear solution, we need to set the value of the eigenfunctions $\varphi_n$ by the formula (2.3) which involves the generalized Laguerre polynomials $L_n^{[\frac{1}{2}]}$ and some other classical mathematical functions: see Appendix E, Maple algorithm 3.

Finally, by (2.5) and since $g_0(t) = g_1(t) = 0$ then

$$g_N^{\ell in}(t,v) = \sum_{n=2}^{N} e^{-\lambda_n t} G_n \varphi_n(v).$$

The approximate value $g_N^{\ell in}(t,v)$ can be computed by the algorithm 7-bis of Appendix E. We consider the solution of the following linear problem

$$\begin{cases} \partial_t g^{\ell in} + \mathcal{L} g^{\ell in} = 0, \\ g^{\ell in}(0,v) = G(v). \end{cases} \tag{3.7}$$

and we estimate the $L^2$ theoretical error $(g^{\ell in} - g_N^{\ell in})$ for different initial data $G$ used for computation in the next sections.

**(i) Cutoff case.** The collision kernel is regular, then from the convergence dominated theorem applied to the integral (2.4), we obtain the following estimate of $\lambda_n$

$$\lambda_n \approx \int_0^{\pi} 2\pi \sin\theta b(\cos\theta)\, d\theta.$$

Therefore, we get for an initial data $G \in L^2$ and when $n$ goes to infinity

$$\|g^{\ell in}(t,\cdot) - g_N^{\ell in}(t,\cdot)\|_{L^2}^2 \lesssim e^{-ct} \sum_{n \geq N+1} |G_n|^2.$$

For a measure initial data, there is no regularization in $L^2$ of the solution for positive time.

**(ii) Non cutoff case.** We study the theoretical rate of convergence of the approximate solution. By the following assumption $b(\cos\theta) \underset{0}{\approx} \frac{1}{|\theta|^{2+2s}}$, we have the following estimate (see [32]) on the linear eigenvalues $\lambda_n$ of $\mathcal{L}$ defined in (2.4)

$$\lambda_n \underset{\infty}{\approx} n^s. \tag{3.8}$$

Therefore, there is a regularization of the solution for positive time and we obtain the following rates of convergence.

PROPOSITION 3.1. *We consider the solution of the linear problem (3.7). Then we have the following estimates:*

*(1) For initial data $G \in L^2$,*

$$\|g^{\ell in}(t,\cdot) - g_N^{\ell in}(t,\cdot)\|_{L^2} \lesssim e^{-cN^s t} \|G\|_{L^2}.$$

*(2) For the measure initial data G defined by (5.1) and $s=\frac{1}{2}$ (see also Proposition C.1), there exist some constants $b>0$ and $\gamma>0$ such that for $t>0$*

$$\|g^{\ell in}(t,\cdot)-g_N^{\ell in}(t,\cdot)\|_{L^2}\lesssim\frac{1}{t^b}e^{-\gamma N^{\frac{1}{2}}t}.$$

*Proof.* The solution of (3.7) is

$$g^{\ell in}(t,v)=\sum_{n=0}^{\infty}e^{-\lambda_n t}G_n\varphi_n(v).$$

From (3.6), the exact error in $L^2$ is

$$\|g^{\ell in}(t,\cdot)-g_N^{\ell in}(t,\cdot)\|_{L^2}^2=\sum_{n=N+1}^{\infty}e^{-2\lambda_n t}|G_n|^2.$$

We first prove (1). If $G\in L^2(\mathbb{R}^3_v)$, then as we have from (3.8)

$$\|g^{\ell in}(t,\cdot)-g_N^{\ell in}(t,\cdot)\|_{L^2}^2=\sum_{n=N+1}^{\infty}e^{-2\lambda_n t}|G_n|^2\lesssim e^{-2cN^{\frac{1}{2}}t}\|G\|_{L^2}^2.$$

We can deduce that the exact error tends to zero when $N$ tends to infinity.

We now prove (2). We suppose now that F is the measure initial data $\mu+\delta$. We can approximate the spectral coefficients $G_n$ of G by $n^{\frac{1}{4}}$ and by (3.8) we can then find some positive constants $c$ and $C$ such that

$$\|g^{\ell in}(t,\cdot)-g_N^{\ell in}(t,\cdot)\|_{L^2}^2\le C\sum_{n=N+1}^{\infty}e^{-cn^{\frac{1}{2}}t}n^{\frac{1}{2}}.$$

We consider the function $\rho_t$ defined on $\mathbb{R}_+$ by $\rho_t(x)=e^{-cx^{\frac{1}{2}}t}x^{\frac{1}{2}}$. So that $\rho_t$ is positive, continuous increasing for $0\le x\le 1/(ct)^2$ and decreasing for $x\ge 1/(ct)^2$, therefore by using the Cauchy integral criterion, we can write the following inequality:

$$\|g^{\ell in}(t,\cdot)-g_N^{\ell in}(t,\cdot)\|_{L^2}\le\frac{C}{t^b}e^{-\gamma N^{\frac{1}{2}}t}\underset{N\to\infty}{\longrightarrow}0$$

where $C$, $b$ and $\gamma$ are some positive constants. ∎

**3.4. Numerical solutions of the nonlinear part.** From (2.9), we consider the approximate solution of the nonlinear part

$$g_N^{n\ell}(t,v)=\sum_{n=0}^{N}e^{-\lambda_n t}h_n(t)\varphi_n(v). \tag{3.9}$$

We compute $h_n(t)$ using the algorithm 6 in Appendix E.

(1) $h_0=h_1=h_2=h_3\equiv 0$

(2) We suppose that for $n\ge 4$ we have computed $h_k(t)$ for $k=0,1,\cdots,n-1$. From Proposition 2.2, $h_k(t)$ is a finite sum of exponential terms $a_ie^{-\alpha_i t}$. Then we compute $h_n(t)$ by the formula (2.8) and the symbolic tool of Maple

$$\texttt{int(function(s), s=0..t)}=\int_0^t\texttt{function}(s)\,ds$$

which consists of integration of exponential terms.

We therefore obtain the following symbolic solutions:

$$h_4 = \frac{\mu_{22}}{\lambda_2+\lambda_2-\lambda_4} {G_2}^2 \left(1-e^{-(\lambda_2+\lambda_2-\lambda_4)t}\right),$$
$$h_5 = \frac{\mu_{23}+\mu_{32}}{\lambda_2+\lambda_3-\lambda_5} G_2 G_3 \left(1-e^{-(\lambda_2+\lambda_3-\lambda_5)t}\right),$$
$$\dots$$

In the algorithm, we assign the numerical values to the variables $G_n$, $\lambda_n$, $\mu_{pq}$ as soon as possible to reduce the lengths of the expressions of $h_n(t)$. For example, in non cutoff case $s=\frac{1}{2}$, we get the numerical approximation:

$$\begin{aligned}
h_0 &= h_1 = h_2 = h_3 = 0,\\
h_4 &= 2.51 {G_2}^2 \left(1-e^{-0.279t}\right),\\
h_5 &= 1.62 G_2 G_3 \left(1-e^{-0.698t}\right),\\
h_6 &= 0.322 {G_3}^2 \left(1-e^{-1.20t}\right) + 1.17 \left(1-e^{-0.928t}\right) G_2 G_4\\
&\quad + \left(-2.95 e^{-0.928t} + 0.677 + 2.26 e^{-1.20t}\right) {G_2}^3,\\
h_7 &= 0.501 G_2 G_5 \left(1-e^{-1.09t}\right) + 0.220 \left(1-e^{-1.51t}\right) G_3 G_4\\
&\quad + \left(0.201 + 0.478 e^{-1.79t} - 0.274 e^{-1.51t} - 0.407 e^{-1.09t}\right) {G_2}^2 G_3,\\
&\dots
\end{aligned}$$

We finally get from (3.9) the approximation $g_N^{n\ell}$ of the nonlinear part of the solution $g^{n\ell}(t,v)$ by the algorithm 7-bis.

REMARK 3.1.

(1) In order to compare the linear part and the nonlinear part, we define the ratio in $L^2$-norm

$$R_N(t) = \frac{\|g_N^{n\ell}(t,\cdot)\|_{L^2_v}}{\|g_N^{\ell in}(t,\cdot)\|_{L^2_v}} = \frac{\left(\sum_{n=4}^N |e^{-\lambda_n t} h_n(t)|^2\right)^{\frac{1}{2}}}{\left(\sum_{n=2}^N |e^{-\lambda_n t} G_n|^2\right)^{\frac{1}{2}}}. \tag{3.10}$$

In the non cutoff case, if we suppose for a small initial data $G$ in $L^2$ that $G_2 \neq 0$ and the solution is regular (which is true from [33]), then the approximation of the series by their first term gives

$$\begin{aligned}
g_N^{\ell in}(t,v) &\approx e^{-\lambda_2 t} G_2 \varphi_2(v),\\
g_N^{n\ell}(t,v) &\approx e^{-\lambda_4 t} h_4(t) = \frac{\mu_{22}}{2\lambda_2-\lambda_4} G_2^2 e^{-\lambda_4 t} (1-e^{-(2\lambda_2-\lambda_4)t}) \varphi_4(v)
\end{aligned}$$

since $\lambda_n \simeq n^s$. Therefore, the ratio $R_N(t)$ can be approximated by

$$R_N(t) \approx \tilde{R}(t) \overset{\text{def}}{=} \frac{\mu_{22}}{2\lambda_2-\lambda_4} |G_2| e^{-(\lambda_4-\lambda_2)t} (1-e^{-(2\lambda_2-\lambda_4)t}). \tag{3.11}$$

For a measure initial data, the previous approximation is no more accurate for small $t$ since the $L^2$ norm of the linear part blows up when $t \to 0$. If we consider the problem for the initial distribution data $\mu+\delta$ where $G_{2n} \approx n^{\frac{1}{4}}$ (see Proposition C.1), we can check that the linear part of the solution is singular

$$\|g^{\ell in}(t,\cdot)\|^2_{L^2} = \sum_{n=2}^{\infty} G_n^2 e^{-2\lambda_n t} \approx \frac{1}{t^\alpha}, \quad \text{when} \quad t \to 0 \tag{3.12}$$

for some $\alpha > 0$.

(2) The length of the symbolic expression $h_n(t)$ increases exponentially with respect to $n$ and therefore by (3.9), the length of $g_N^{n\ell}(t,v)$ blows up: $h_{40}$ has 7355 exponential terms $a_i e^{-\beta_i t}$ and $g_{40}^{n\ell}(t,v)$ has $1.6\times 10^6$ exponential polynomial terms $a_i v^{n_i} e^{-\beta_i t}$ after expanding the expression of $g_{40}^{n\ell}(t,v)$ with the Maple tool `expand(expression)`. We present in Figure 3.1 the evolution of the number of terms of $h_n(t)$ and $g_n^{n\ell}(t,v)$ for $n=4,\dots,N=40$.

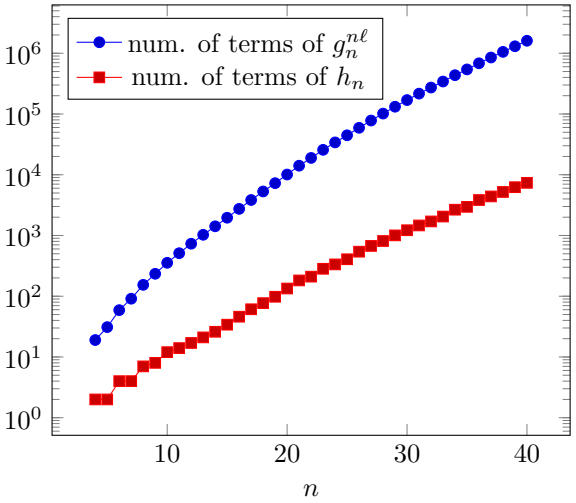


FIG. 3.1. *Number of terms of the approximate solution*

The symbolic and numerical computation of the nonlinear part $h_n(t)$ play the major role of our method with respect to cost in time and storage. We analyze the computation time and rounding off error in the next section.

## 4. Spectral computation of the BKW solution

In this section, we give a numerical example of exact solutions (we take the BKW solution in the cutoff and non cutoff case) and we test the accuracy of the method using these solutions. In the cutoff case, the initial data is represented by a small $L^2$ initial condition. In the non cutoff case, it is represented by an initial distribution data.

**4.1. Numerical results for the cutoff case.** We study the specific case of a constant kernel (1.2) and the spectral approximation of the BKW solution (3.4) (see also Appendix A). In [23], the authors test their numerical method for a time $t\in[5.5,6.5]$ to get a positive solution. For that, we assume that $t_0=5.5$ is the initial time and $t_1=6.5$ is the final time. So we consider the following initial condition

$$F(v)=f_{\text{BKW}}(t_0,v).$$

We show in the Figure 4.1 the spectral approximation $F_N(v)$ of the initial data $F(v)$ (see (3.2)). We next compute the nonlinear solutions $h_n(t)$ of the Proposition 2.1 for $n=4,5,\dots,N$ with $N=40$. For each integer $n$, the function $t\to h_n(t)$ is monotone and tends to a finite limit when $t$ goes to infinity, see Figure 4.2. We recall that $h_n(t)$ is a finite sum of decreasing exponential terms, see Proposition 2.2. In the special case of the BKW solution, we have computed the exact values of $h_n(t)$, see Proposition A.2. Since the initial data $G$ is a regular function, the spectral coefficients $G_n$ decrease

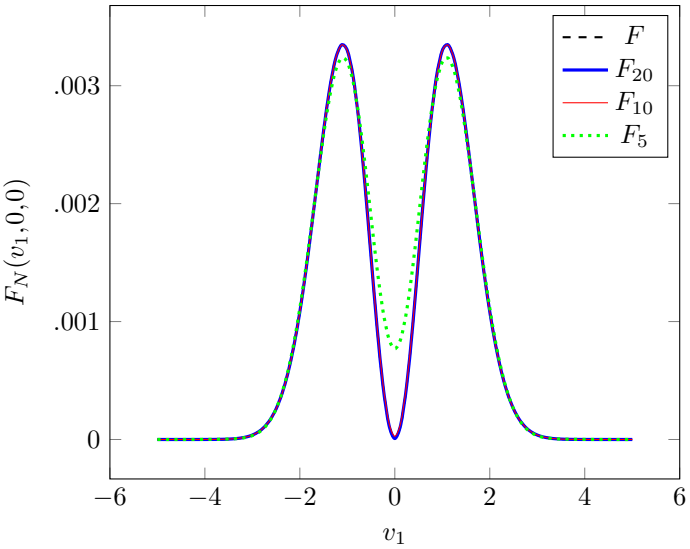


FIG. 4.1. *Approximation of the initial data of the BKW solution.*

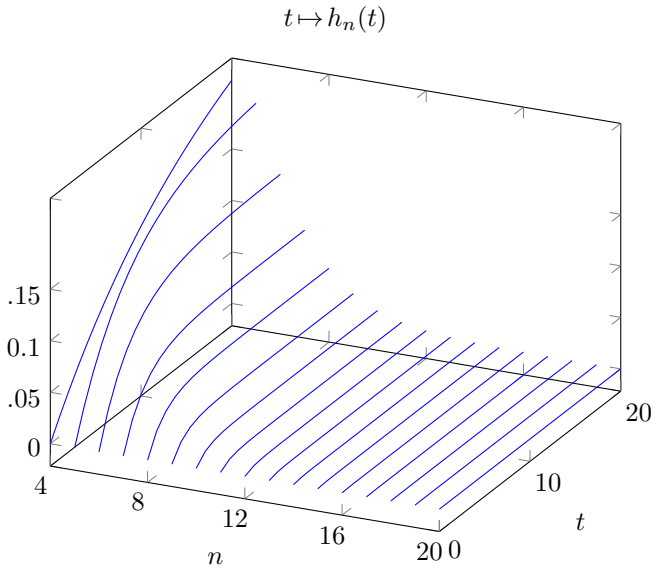


FIG. 4.2. *Behavior of the nonlinear solution $h_n$.*

exponentially. We can check from Proposition A.3 and the Stirling's formula that $G_n \approx n^{\frac{5}{4}} e^{-nt_0/6}$.

Finally, using the algorithm 8 in Appendix E, we calculate the relative error

$$E_N(t) = \frac{\|f_N(t,\cdot) - f_{\text{BKW}}(t,\cdot)\|_{L^\infty_v}}{\|f_{\text{BKW}}(t,\cdot)\|_{L^\infty_v}}$$

between the spectral approximate solution $f_N$ and the BKW solution at time $t_0$ and $t_1$ and for different significant digits: 5, 10, 20. We present this error $E_N(t)$ at time $t_0$ and $t_1$ in Figure 4.3, and the final error at time $t_1$ in Table 4.1. We remark that the

accuracy at time $t_1$ is better than at time $t_0$. We can explain this because of a fast regularization effect in time of the solution $f(t,\cdot)$. For our numerical analysis, we will focus on the final time $t_1$. More precisely:

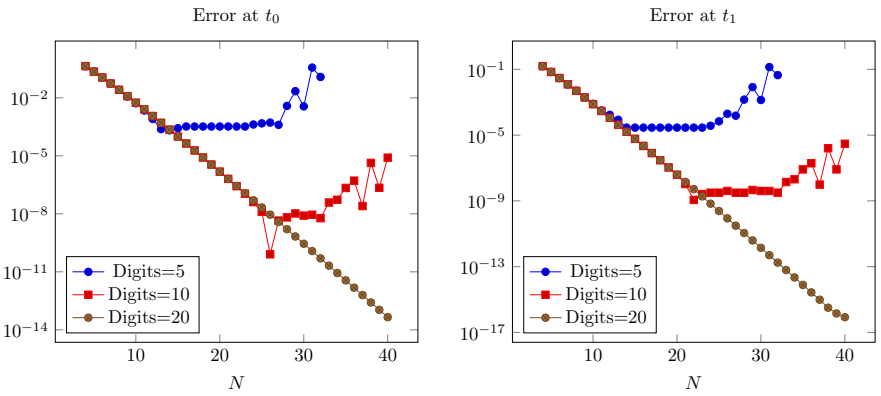


FIG. 4.3. *Relative error $E_N(t)$ in $L^\infty_v$ between $f_N(t,\cdot)$ and $f_{BKW}(t,\cdot)$.*

| N | Digits=5 | Digits=10 | Digits=20 |
|---|---|---|---|
| 5 | 7.0e-02 | 7.0e-02 | 7.0e-02 |
| 10 | 8.9e-04 | 7.7e-04 | 7.7e-04 |
| 15 | 8.6e-05 | 6.0e-06 | 6.0e-06 |
| 20 | 8.6e-05 | 3.8e-08 | 4.0e-08 |
| 25 | 3.2e-04 | 4.0e-09 | 2.5e-10 |
| 30 | 3.7e-02 | 4.0e-09 | 1.4e-12 |
| 35 | 1.4e+01 | 8.2e-08 | 7.8e-15 |
| 40 | 2.0e+03 | 3.0e-06 | 8.5e-17 |

TABLE 4.1. *Relative error $E_N(t_1)$ in $L^\infty_v$ between $f_N(t_1,\cdot)$ and $f_{BKW}(t_1,\cdot)$.*

- From the Table 4.1, we conclude that for a given (large enough) digits and for large $N$, we have $E_N \approx 6.3\times 10^{-0.42N}$.
- To have a relative precision of $10^{-5}$, just choose the degree of freedom $N=15$ and set the software's accuracy to 5, 10 or 20 significant digits. But in the case of Digits $=5$, do not take $N$ big: indeed, from N $=15$, the exact error stabilizes, and even increases starting at $N=25$.
- For an accuracy of $10^{-10}$, the precision Digits $=5$ is no longer valid. We can choose Digits $=10$ or 20, but limit to $N=23$ in the case of Digits $=10$, because the error stagnates.
- To have a precision around $10^{-17}$, we have to set the software to Digits $=20$ and choose $N=40$. But we point out that the duration time lengthens rapidly and exponentially. It is here approximated for $N\in[30,40]$ by $0.0407\times 10^{0.146N}$ (see Table 4.2).
- We notice that the computing time is about the same for numerical accuracy of the Maple software set to 5 or 10 significant digits, but is different for 20 significant digits (see the left Figure 4.4).

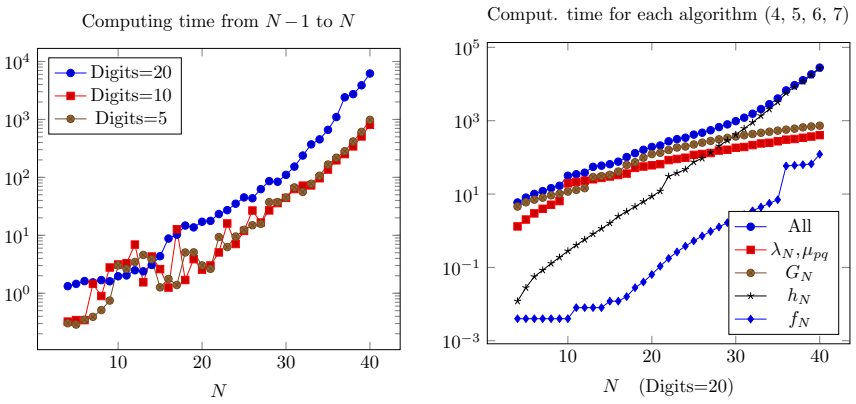


FIG. 4.4. *Computing time (in seconds)*

- For large $N$ ($N \geq 30$), the main part of the computing time is devoted to calculate the nonlinear part $h_n(t)$ (see the right Figure 4.4).
- We compare our numerical results (see Table 4.2) with (for example) the results of Gamba et al. [23] (see Section 4.1) where the authors have tested their fast spectral method on the BKW solution at the same time [5.5,6.5]. They have obtained, for a degree of freedom $N = 32$, an error of 3.90e-08 (time=1.78s) and an error of 3.81e-08 (time=33.15s) for $N = 64$. We point out that our method is limited to radial solutions. But it can be generalized to non-radial solutions using the spherical harmonics (see [24] and the associated references).

| N | 10 | 20 | 30 | 40 |
|---|---|---|---|---|
| CPU time (s) | 31. | 192. | 973. | 28007. |
| Error $E_N(t_1)$ | 7.7e-04 | 4.0e-08 | 1.4e-12 | 8.5e-17 |

TABLE 4.2. *CPU time and error of all algorithms for Digits=20, cutoff case.*

**4.2. Numerical results for the non cutoff case.** We test our method in the non cutoff case. We remark that if we set the collision kernel (non cutoff case (3.5) with $s = \frac{1}{2}$)

$$2\pi \sin\theta\, b(\cos\theta) = \begin{cases} \frac{2}{6+3\pi} \sin^{-2}\left(\frac{\theta}{2}\right) & \text{if} \quad \theta \in [0, \frac{\pi}{2}[, \\ 0 \quad \text{if} \quad \theta \in [\frac{\pi}{2}, \pi]. \end{cases}$$

then the constant defined in (A.1) is $\bar{B} = \frac{1}{6}$, and choosing again $\beta_0 = -\frac{1}{2}$, we derive exactly the same explicit BKW solution (3.4) which was tested in the previous section. But note that the eigenvalues $\lambda_n$ and $\mu_{pq}$ are completely different. For $t \geq 5.5$, this solution is positive and tends to the Maxwellian distribution as $t$ goes to infinity. We compare the approximated solution with this BKW solution and we test the accuracy of the method. Note that for $t = 0$, the initial data $F = f_{\text{BKW}}(0, \cdot)$ is a sign-changing distribution whose Fourier transform is

$$\mathcal{F}(F)(\xi) = 1 - \frac{1}{2}|\xi|^2$$

and the spectral coefficients of $G=(F-\mu)/\sqrt{\mu}$ are given in Proposition A.2 by

$$G_n=\frac{-(n-1)\sqrt{(2n+1)!}}{2^n n!}. \tag{4.1}$$

We can check with the Stirling's formula that $G_n\approx n^{\frac{5}{4}}$ so that we can also test the method with a distribution initial data. Therefore, we have set directly in the Algorithm 5 the spectral coefficients $G_n$ by the formula (4.1). Remark that the solution BKW changes sign for $t<5.5$. We get roughly the same results as in Section 4.1, see Table 4.2 and 4.3. The difference in time comes from the difference in the collision kernel.

| N | 10 | 20 | 30 | 40 |
|---|---|---|---|---|
| CPU time (s) | 3.2 | 33. | 570. | 35924. |
| Error $E_N(t_1)$ | 7.6e-04 | 4.0e-08 | 1.4e-12 | 4.2e-17 |

TABLE 4.3. *CPU time and error of all algorithms for Digits=20, non cutoff case.*

## 5. Numerical results for initial measure data

We apply in this section the previous symbolic and numerical codes to calculate the solution for the positive initial measure data

$$\tilde{F}=(\text{Maxwellian distribution})+\text{Dirac}=\mu+\delta.$$

We consider only the non cutoff case, since there is some regularization in time. We have tested the algorithm for an explicit BKW solution for a sign-changing distribution initial data. Following the Lemma B.1 and rescaling the solution $F(v)=2^{-\frac{5}{2}}\tilde{F}(2^{-\frac{1}{2}}v)$, we get the normalized initial data

$$\begin{cases} F(v)=2^{-\frac{5}{2}}\mu(2^{-\frac{1}{2}}v)+2^{-1}\delta(v), \\ G(v)=2^{-\frac{13}{4}}\pi^{-\frac{3}{4}}-\sqrt{\mu(v)}+2^{-\frac{1}{4}}\pi^{\frac{3}{4}}\delta(v). \end{cases} \tag{5.1}$$

We verify that $\langle G,\varphi_0\rangle=\langle G,\varphi_1\rangle=0$ and therefore $G\in\mathcal{N}^{\perp}$. We then compute the spectral coefficients for $n\geq 0$ (see Proposition C.1)

$$G_n=\langle G,\varphi_n\rangle=\frac{1+(-1)^n}{2}\left(\frac{(2n+1)!}{2^{2n}(n!)^2}\right)^{\frac{1}{2}}.$$

Note that the coefficients $G_{2n+1}$ are equal to zero and we have from the Stirling's formula the following approximation of $G$

$$G(v)\approx\sum_{n=1}^{\infty}n^{\frac{1}{4}}\varphi_{2n}(v).$$

We set $F_{\text{reg}}(v)=2^{-\frac{5}{2}}\mu(2^{-\frac{1}{2}}v)$ as the regular part of the distribution $F$. We check in the left Figure 5.1 that the approximate initial data behaves as a Dirac function.

Remark that to capture the approximation of the regular part $F_{\text{reg}}$, we have to rescale the $y$-axis. We observe the oscillations of $F_N$, which are expected since the functions $F_N$ approach the Dirac function when $N$ tends to infinity (see the right Figure 5.1). We now focus on the evolution problem. We next compute the nonlinear part $h_n(t)$ of the solution (see Figure 5.2).

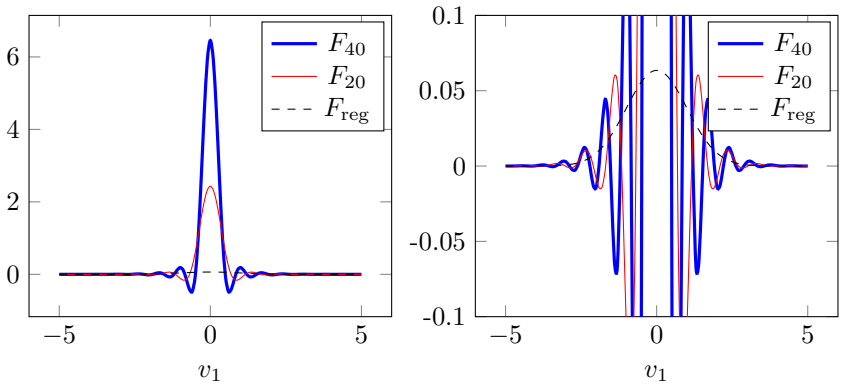


FIG. 5.1. *Approximation of the initial data* $v_1 \to F_N(v_1,0,0)$.

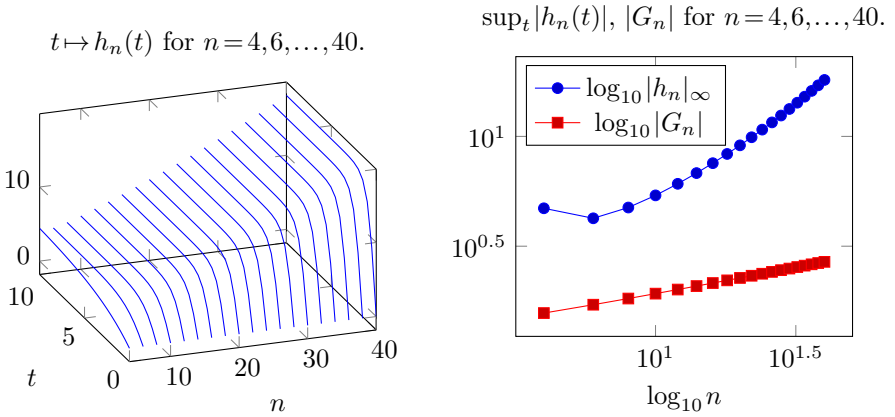


FIG. 5.2. *Behavior of the nonlinear part* $h_n$.

We observe some numerical evidences that these functions are increasing less than some power of $n$

$$\sup_{t\geq 0}|h_n(t)| \leq C n^a$$

with $a$ close to 1. Since $G_{2n} \approx n^{\frac{1}{4}}$, the behavior of a term of the series $(g_N^{\ell in}(t) + g_N^{n\ell}(t))$ is dominated by the linear part: we can check this observation by computing the ratio $R_N(t) = \|g_N^{n\ell}(t,\cdot)\|_{L^2} / \|g_N^{\ell in}(t,\cdot)\|_{L^2}$ defined in (3.10) (see Figure 5.3). The numerical computations in the left figure show that $g_N^{n\ell}(t)$ is a regular function for all time. For small time, we verify that $g_N^{\ell in}(t)$ is singular as $t \to 0$ as pointed in (3.12). For a large time, the $L^2$ norm of the linear part $(\sim e^{-\lambda_2 t})$ dominates the norm of the nonlinear part $(\sim e^{-\lambda_4 t})$ and the ratio $R_N(t)$ behaves as $\tilde{R}(t)$, see (3.11).

We then compute the numerical approximation $f_N$ of the solution $f$ for $N = 40$ and we check that the solution behaves as a Dirac function as $t \to 0$ and tends to the Maxwellian distribution as $t \to \infty$ (see Figure 5.4). Since $\lambda_n \approx c\sqrt{n}$ and if the behavior of $\sup_{t\geq 0}|h_n(t)|$ is dominated by some power of $n$ (which is numerically verified), then

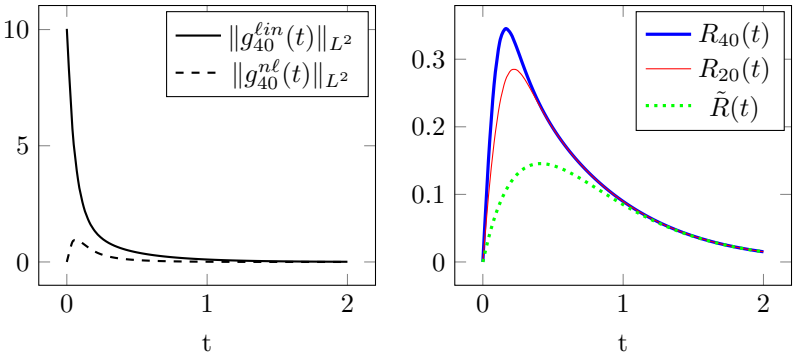


FIG. 5.3. *Graph of the linear part, nonlinear part and the ratio* $R_N(t) = \frac{\|g_N^{n\ell}(t,\cdot)\|_{L^2_v}}{\|g_N^{\ell in}(t,\cdot)\|_{L^2_v}}$.

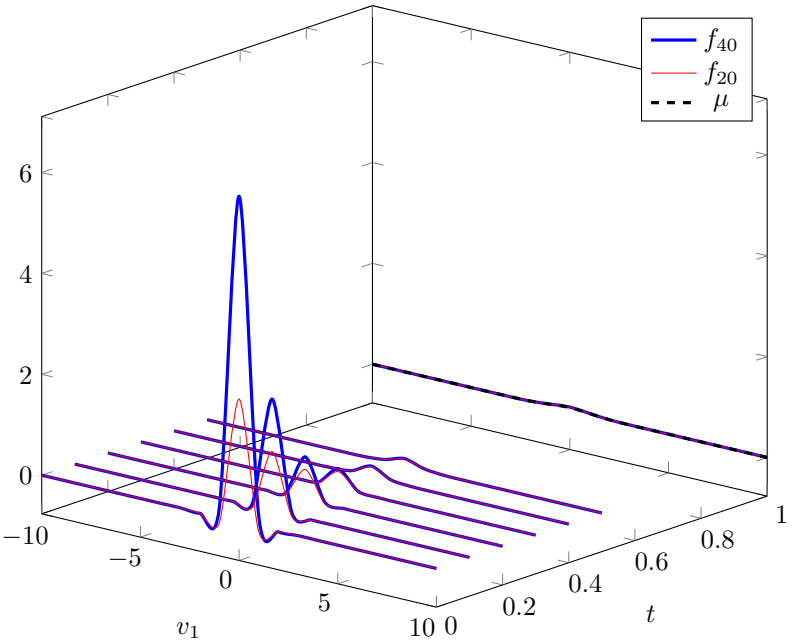


FIG. 5.4. *Graph of* $(t,v_1) \mapsto f_N(t,v_1,0,0)$ *for* $N = 20,\ 40$ *and* $\mu(v_1,0,0)$.

we have for some $b, \gamma > 0$

$$\forall t > 0,\ \|(f_N(t,\cdot) - f(t,\cdot))/\sqrt{\mu}\|_{L^2} \lesssim \frac{1}{t^b} e^{-\gamma\sqrt{N}t} \to 0 \quad \text{as} \quad N \to \infty.$$

The previous numerical observations suggest that the series $(g_N^{\ell in}(t) + g_N^{n\ell}(t))$ converges in $L^2$ for $t > 0$ and the solution $f(t,\cdot)$ converges to a Maxwellian distribution as $t \to \infty$.

## 6. Conclusion

We have considered the perturbation $g$ of the solution $f$ of the Boltzmann equation

defined by

$$f=\mu+\sqrt{\mu}g \quad \text{where} \quad g(t,v)=\sum_n g_n(t)\varphi_n(v)$$

and we have studied the behavior of the spectral coefficients

$$g_n(t)=e^{-\lambda_n t}(G_n+h_n(t)), \quad g_n(0)=G_n.$$

We have then computed formally the spectral coefficients $h_n(t)$ for $n=0,1,\dots,N$ with $N=40$. We have considered the case of the BKW solution and the case of the distribution-type initial data $\mu+\delta$:

- We have tested the algorithms with the explicit BKW solution in both cases (cutoff and non cutoff). In the cutoff case, we have deduced that the relative error between the approximated solution and the BKW solution is exponentially decreasing ($E_N \approx 6.3\times 10^{-0.42N}$) with respect to the degree of freedom $N$. The CPU time is exponentially increasing with respect to $N$ ($0.0407\times 10^{0.146N}$). Moreover, it is increasing as long as the significant digit increases. The computing time shows that the nonlinear part $h_n(t)$ and the initial data $G_n$ take most of the time. Note that we have obtained the same results in the non cutoff case.
- We have computed in the non cutoff case the solution for the distribution initial data $\mu+\delta$. The simulations show some numerical evidences that for all positive time the spectral series converges in $L^2_v$. On the other hand, the nonlinear part $g^{n\ell}$ stays uniformly bounded in time in $L^2_v$. Moreover, there is a regularization in time of the solution for $t>0$.

We have computed the formal solutions of the spectral coefficients $h_n(t)$ related to the solution of the Boltzmann equation and we get the exact values for the special collision kernels cutoff (3.3) and non cutoff (3.5) with $s=\frac{1}{2}$. The numerical results are coherent for small $L^2_v$ initial data or for the distribution case $\mu+\delta$. There is conservation of the mass, momentum and energy of the approximated solution since $g(t,\cdot)$ is orthogonal to the kernel $\mathcal{N}$ for all time, see Remark 2.1. Moreover the approximated solution $f_N(t,\cdot)$ defined in (3.1) converges to a Maxwellian distribution when $t$ goes to infinity.

**Acknowledgments.** The authors wish to thank Chao-Jiang Xu for interesting discussions. They also gratefully acknowledge the referees for their constructive input. This project was co-financed by the European Union with the European regional development fund (ERDF, HN0002137) and by the Normandie Regional Council via the M2NUM project.

**Appendix A. On the BKW solution.** We recall the definition of the BKW solution.

PROPOSITION A.1. *[4, 30] We note $\bar{B}$ the positive real which is defined from the Boltzmann kernel*

$$\bar{B}=\int_0^\pi 2\pi\sin\theta\, b(\cos\theta)\left\{\cos^2\left(\frac{\theta}{2}\right)\sin^2\left(\frac{\theta}{2}\right)\right\}d\theta \tag{A.1}$$

*and we consider for a given real $\beta_0$ the function*

$$f_{BKW}(t,v)=\frac{1}{(2\pi)^{\frac{3}{2}}}\frac{1}{(1+2\beta(t))^{\frac{7}{2}}}\left[(1+5\beta(t))(1+2\beta(t))-\beta(t)|v|^2\right]e^{-\frac{|v|^2}{2+4\beta(t)}}$$

*where* $\beta(t)=\beta_0 e^{-\bar{B}t}$. *Then the Fourier transform is given by*

$$\widehat{f_{BKW}}(t,\xi)=e^{-(\frac{1}{2}+\beta(t))|\xi|^2}+\beta(t)|\xi|^2 e^{-(\frac{1}{2}+\beta(t))|\xi|^2}$$

*and the function* $f_{BKW}(t,v)$ *is a solution of the Boltzmann equation.*

REMARK A.1. Following [30] and the associated references, if we choose $b(\cos\theta)\equiv\frac{1}{4\pi}$ and $\beta(0)=-\frac{1}{2}$, we get $\bar{B}=\frac{1}{6}$, $\beta(t)=-\frac{1}{2}e^{-t/6}$, and the BKW solution given in (3.4).

*Proof.* (Proof of Proposition A.1.) We follow the proof of [16]. We are looking for a radial solution of the form

$$\hat{f}(t,\xi)=c(1+\beta(t)|\xi|^2)e^{-(\alpha+\beta(t))|\xi|^2},\quad \alpha,c>0.$$

Then

$$\partial_t\hat{f}(t,\xi)=-c\beta(t)\beta'(t)|\xi|^4 e^{-(\alpha+\beta(t))|\xi|^2}. \tag{A.2}$$

To compute the collision term $\mathcal{F}(Q(f,f)(v))(\xi)$, we use the Bobylev identity

$$\mathcal{F}[Q(f,f)(t,\cdot)](\xi)=\int_{\mathbb{S}^{N-1}} b\left(\frac{\xi}{|\xi|}\cdot\sigma\right)\left\{\hat{f}(t,\xi^-)\hat{f}(t,\xi^+)-\hat{f}(t,0)\hat{f}(t,\xi)\right\}d\sigma$$

where $\mathcal{F}(f)(\xi)=\int e^{-i\xi\cdot v}f(v)dv$ and $\xi^+$ and $\xi^-$ are defined by

$$\xi^+=\frac{\xi+|\xi|\sigma}{2},\quad \xi^-=\frac{\xi-|\xi|\sigma}{2}.$$

If we set $\xi=(|\xi|,0,0)$ and $\sigma=(\cos\theta,\sin\theta\cos\phi,\sin\theta\sin\phi)$, we can verify that

$$|\xi^+|=|\xi||\cos(\theta/2)|,\quad |\xi^-|=|\xi||\sin(\theta/2)|$$

and

$$\begin{aligned}\left\{\hat{f}(t,\xi^-)\hat{f}(t,\xi^+)-\hat{f}(t,0)\hat{f}(t,\xi)\right\}&=c^2\left\{(1+\beta|\xi^-|^2)(1+\beta|\xi^+|^2)-(1+\beta|\xi|^2)\right\}e^{-(\alpha+\beta)|\xi|^2}\\&=c^2\beta^2|\xi^-|^2|\xi^+|^2e^{-(\alpha+\beta)|\xi|^2}.\end{aligned}$$

Therefore, from the Bolylev identity, we have

$$\mathcal{F}[Q(f,f)(t,\cdot)](\xi)=\bar{B}\times c^2\beta(t)^2|\xi|^4e^{-(\alpha+\beta(t))|\xi|^2}$$

where $\bar{B}$ is defined in (A.1). Finally, we compare the previous identity with (A.2), we get the ODE on $\beta(t)$

$$\beta'(t)=-c\bar{B}\beta(t).$$

Therefore $\beta(t)=\beta(0)e^{-c\bar{B}t}$. ∎

We compute the exact coefficient of the BKW solution in the spectral basis.

PROPOSITION A.2. *We consider the BKW solution* (3.4) *defined in Remark A.1. Then we have the following expansion in the spectral basis*

$$f(t,v)=\mu(v)+\sqrt{\mu(v)}\left(g_2(t)\varphi_2(v)+\cdots+g_n(t)\varphi_n(v)+\cdots\right)$$

*where for* $n \geq 2$

$$g_n(t) = \frac{-(n-1)\sqrt{(2n+1)!}}{2^n n!} e^{-\frac{nt}{6}}.$$

*Proof.* We consider the Fourier transform of the BKW solution where $\beta(t) = -\frac{1}{2}e^{-t/6}$

$$\widehat{f}(t,\xi) = \left(1 - \frac{1}{2}e^{-\frac{t}{6}}|\xi|^2\right) e^{-(1-e^{-\frac{t}{6}})\frac{|\xi|^2}{2}}.$$

We set $a = \frac{1}{2}e^{-\frac{t}{6}}$ so that

$$\begin{aligned}\widehat{f}(t,\xi) &= \left(e^{a|\xi|^2} - a|\xi|^2 e^{a|\xi|^2}\right) e^{-\frac{|\xi|^2}{2}} \\ &= \left(1 + \frac{a}{1!}|\xi|^2 + \cdots + \frac{a^n}{n!}|\xi|^{2n} + \cdots - a|\xi|^2 - \cdots - \frac{a^n}{(n-1)!}|\xi|^{2n} - \cdots\right) e^{-\frac{|\xi|^2}{2}}.\end{aligned}$$

Since $\frac{a^n}{n!} - \frac{a^n}{(n-1)!} = \frac{a^n(1-n)}{n!}$, we get

$$\widehat{f}(t,\xi) = \left(1 - \frac{a^2}{2}|\xi|^4 - \cdots - \frac{(n-1)a^n}{n!}|\xi|^{2n} - \cdots\right) e^{-\frac{|\xi|^2}{2}}.$$

Then comparing to the expansion in the spectral basis $\mathcal{F}(\varphi_n)(\xi) = \frac{|\xi|^{2n}}{\sqrt{(2n+1)!}}$ (see [32])

$$\widehat{f}(t,\xi) = \left(1 + \frac{g_2(t)}{\sqrt{5!}}|\xi|^4 + \cdots + \frac{g_n(t)}{\sqrt{(2n+1)!}}|\xi|^{2n} + \cdots\right) e^{-\frac{|\xi|^2}{2}},$$

we get the value of $g_n(t)$. ∎

The eigenvalues of the Boltzmann operators have explicit expressions.

PROPOSITION A.3. *We suppose that* $b(\cos\theta) \equiv \frac{1}{4\pi}$ *on all* $[0,\pi]$. *We have the following formulas*

*(i)* $\lambda_0 = 0$ *and for all* $n \geq 1$ *we have* $\lambda_n = \frac{n-1}{n+1}$.

*(ii) For all* $q \geq 0$, $\mu_{0q} = -\frac{q}{q+1}$.

*(iii) For all* $p \geq 1$ *and* $q \geq 0$, $\mu_{pq} = \left(\frac{(2p+2q+1)!}{(2p+1)!(2q+1)!}\right)^{\frac{1}{2}} \frac{p!q!}{(p+q+1)!}$.

*Proof.* We first compute $\lambda_n$ where

$$\lambda_n = \int_0^\pi \frac{1}{2}\sin\theta \left\{1 - \cos^{2n}\left(\frac{\theta}{2}\right) - \sin^{2n}\left(\frac{\theta}{2}\right)\right\} d\theta.$$

We pose $x = \cos^2\frac{\theta}{2}$ and we easily get

$$\lambda_n = \int_0^1 (1 - x^n - (1-x)^n)\, dx = \frac{n-1}{n+1}.$$

We then compute $\mu_{0q}$ and $\mu_{pq}$: from the same previous change of variable, we have

$$\mu_{0q} = -\int_0^\pi \frac{1}{2}\sin\theta \left\{1 - \cos^{2q}\left(\frac{\theta}{2}\right)\right\} d\theta = -\int_0^1 (1 - x^q)\, dx = -\frac{q}{q+1}$$

and by the classical formula of the beta function, $\mu_{pq} = \left(\frac{(2p+2q+1)!}{(2p+1)!\,(2q+1)!}\right)^{\frac{1}{2}} M_{pq}$ where

$$M_{pq} = \int_0^\pi \frac{1}{2}\sin\theta \left\{\sin^{2p}\left(\frac{\theta}{2}\right)\cos^{2q}\left(\frac{\theta}{2}\right)\right\} d\theta = \int_0^1 (1-x)^p x^q\, dx = B(q+1,p+1).$$

□

**Appendix B. Rescaling of the solution.** We consider a radial solution $\tilde{f}(s,w)$ of the Boltzmann equation

$$\begin{cases} \partial_s \tilde{f} = \mathbf{Q}(\tilde{f},\tilde{f}), \\ \tilde{f}|_{t=0} = \tilde{F}. \end{cases}$$

LEMMA B.1. *We consider the functions $f(t,v)$ and $F(v)$ defined by the change of variable*

$$f(t,v) = \alpha\tilde{f}\left(\frac{\alpha}{\beta^3}t, \beta v\right) \quad \text{and} \quad F(v) = \alpha\tilde{F}(\beta v)$$

*where*

$$\alpha = \frac{\left(\frac{1}{3}\int_{\mathbb{R}^3} w^2\,\tilde{F}(w)\,dw\right)^{\frac{3}{2}}}{\left(\int_{\mathbb{R}^3}\tilde{F}(w)\,dw\right)^{\frac{5}{2}}} \quad \text{and} \quad \beta = \frac{\left(\frac{1}{3}\int_{\mathbb{R}^3} w^2\,\tilde{F}(w)\,dw\right)^{\frac{1}{2}}}{\left(\int_{\mathbb{R}^3}\tilde{F}(w)\,dw\right)^{\frac{1}{2}}}.$$

*Therefore $f(t,v)$ is a solution of the Boltzmann equation (1.1) with initial data $F$. Moreover, if we set $F = \mu + \sqrt{\mu}G$, we then have $G \in \mathcal{N}^\perp$.*

REMARK B.1. If $F$ is such that

$$\int_{\mathbb{R}^3} F(v)\,dv = \int_{\mathbb{R}^3} \mu(v)\,dv = 1,$$
$$\int_{\mathbb{R}^3} v^2 F(v)\,dv = \int_{\mathbb{R}^3} v^2\mu(v)\,dv = 3$$

then the function $G$ defined by $G = \frac{1}{\sqrt{\mu}}(F-\mu)$ belongs to $\mathcal{N}^\perp$.

*Proof.* It is easy to check that $f(t,v)$ is a solution of the Boltzmann equation. Since $G$ is a radial function, it is enough to check that

$$\left(G, \sqrt{\mu}\right)_{L^2} = \left(G, |v|^2\sqrt{\mu}\right)_{L^2} = 0.$$

Recalling that

$$\begin{cases} \left(\varphi_p, \varphi_q\right)_{L^2} = \delta_{pq}, \\ \varphi_0 = \sqrt{\mu} \quad \text{and} \quad \varphi_1 = 6^{-\frac{1}{2}}(3-|v|^2)\sqrt{\mu}. \end{cases}$$

It is equivalent to prove that

$$(F/\sqrt{\mu}, \varphi_0)_{L^2} = 1 \quad \text{and} \quad (F/\sqrt{\mu}, \varphi_1)_{L^2} = 0$$

which gives the equations

$$\begin{cases} \int_{\mathbb{R}^3} F(v)\,dv = \int_{\mathbb{R}^3} \mu(v)\,dv = 1, \\ \int_{\mathbb{R}^3} |v|^2 F(v)\,dv = \int_{\mathbb{R}^3} |v|^2 \mu(v)\,dv = 3. \end{cases}$$

Using the change of variable $w = \beta v$, we can check that if we set the values of $\alpha$ and $\beta$ given in the lemma, the previous equations are fulfilled. ∎

**Appendix C. Measure initial data.** We define the following distribution initial data:

$$\tilde{F} = \mu + \delta.$$

Following the rescaling of Lemma B.1, we compute

$$\langle \tilde{F}, 1 \rangle = \int_{\mathbb{R}^3} \mu(v)\,1\,dv + \langle \delta, 1 \rangle = 2,$$
$$\langle \tilde{F}, v^2 \rangle = \frac{1}{3} \int_{\mathbb{R}^3} \mu(v)\,v^2\,dv + \langle \delta, v^2 \rangle = 1$$

and then $\alpha = 2^{-\frac{5}{2}}$ and $\beta = 2^{-\frac{1}{2}}$. Using the change of variable $w = \beta v$, we get the new rescaled distribution initial data

$$F = \alpha \tilde{F} \circ (\beta \mathrm{Id}) = 2^{-\frac{5}{2}} \left( \mu(2^{-\frac{1}{2}} \cdot) + (2^{\frac{1}{2}})^3 \delta \right).$$

PROPOSITION C.1. *We consider the initial data*

$$F = 2^{-\frac{5}{2}} \left( \mu(2^{-\frac{1}{2}} \cdot) + (2^{\frac{1}{2}})^3 \delta \right)$$

*and we set $G$ such that $F = \mu + \sqrt{\mu} G$. Then $G \in \mathcal{N}^\perp$ and we have*

$$G = -\sqrt{\mu} + 2^{-\frac{13}{4}} \pi^{-\frac{3}{4}} + 2^{-\frac{1}{4}} \pi^{\frac{3}{4}} \delta.$$

*We consider the coordinates $G_n = \langle G, \varphi_n \rangle$ of the distribution $G$ in the spectral basis $(\varphi_n)_n$. We can check that*

$$G_0 = G_1 = 0$$

*and for all integer $n \geq 2$*

$$G_n = \langle G, \varphi_n \rangle = \frac{1 + (-1)^n}{2} \left( \frac{(2n+1)!}{2^{2n} (n!)^2} \right)^{\frac{1}{2}}. \tag{C.1}$$

*Proof.* The expression of $G$ follows from the definition of the Maxwellian distribution $\mu$. We then compute

$$\langle G, \varphi_n \rangle = -(\varphi_0, \varphi_n)_{L^2} + 2^{-\frac{13}{4}} \pi^{-\frac{3}{4}} (1, \varphi_n)_{L^2} + 2^{-\frac{1}{4}} \pi^{\frac{3}{4}} \varphi_n(0)$$

and the conclusion results directly from Lemma D.1. ∎

We consider now a special Maxwellian approximation $F_\varepsilon \in L^2$ of the distribution initial data $F = \mu + \delta$ and we obtain some spectral stability result in this case.

PROPOSITION C.2. *We consider the initial data for* $\varepsilon>0$

$$\tilde{F}_\varepsilon(w)=\mu(w)+\frac{1}{\varepsilon^3}\mu\left(\frac{w}{\varepsilon}\right).$$

*Following Lemma B.1, the rescaled initial data of* $\tilde{F}_\varepsilon$ *is* $F_\varepsilon=\mu+\sqrt{\mu}G_\varepsilon$ *where* $G_\varepsilon\in\mathcal{N}^\perp$ *and*

$$G_\varepsilon(v)=-\sqrt{\mu(v)}+2^{-\frac{5}{2}}\left(1+\varepsilon^2\right)^{3/2}\left(\sqrt{\mu(\varepsilon v)}+\frac{1}{\varepsilon^3}\sqrt{\mu(v/\varepsilon)}\right).$$

*Then we have, when* $\varepsilon$ *goes to zero, the following limit in the sense of distribution*

$$F_\varepsilon\to F=2^{-\frac{5}{2}}\left(\mu(2^{-\frac{1}{2}}\cdot)+(2^{\frac{1}{2}})^3\delta\right),$$
$$G_\varepsilon\to G=-\sqrt{\mu}+2^{-\frac{13}{4}}\pi^{-\frac{3}{4}}+2^{-\frac{1}{4}}\pi^{\frac{3}{4}}\delta.$$

*The coordinates of* $G_\varepsilon$ *in the spectral basis* $(\varphi_n)_{n\geq 0}$ *are given by*

$$G_{\varepsilon,0}=G_{\varepsilon,1}=0,$$
$$G_{\varepsilon,n}=\frac{1+(-1)^n}{2}\frac{\left(1-\varepsilon^2\right)^n}{\left(1+\varepsilon^2\right)^n}\left(\frac{(2n+1)!}{2^{2n}(n!)^2}\right)^{\frac{1}{2}},\quad\forall n\geq 2.$$

*Moreover we have* $G_{\varepsilon,n}\to G_n$ *as* $\varepsilon$ *tends to 0 as* $\varepsilon\to 0$ *where* $G_n$ *is given in* (C.1).

REMARK C.1. There is continuity of the spectral coefficients: $G_{\varepsilon,n}\to G_n$ as $\varepsilon$ tends to 0.

*Proof.* From Lemma B.1, we set

$$F_\varepsilon(v)=\alpha_\varepsilon\tilde{F}_\varepsilon(\beta_\varepsilon v)$$

where

$$\alpha_\varepsilon=\frac{\left(\frac{1}{3}\int_{\mathbb{R}^3}w^2\tilde{F}_\varepsilon(w)\,dw\right)^{\frac{3}{2}}}{\left(\int_{\mathbb{R}^3}\tilde{F}_\varepsilon(w)\,dw\right)^{\frac{5}{2}}}=\frac{\sqrt{2}}{8}\left(1+\varepsilon^2\right)^{3/2},$$
$$\beta_\varepsilon=\frac{\left(\frac{1}{3}\int_{\mathbb{R}^3}w^2\tilde{F}_\varepsilon(w)\,dw\right)^{\frac{1}{2}}}{\left(\int_{\mathbb{R}^3}\tilde{F}_\varepsilon(w)\,dw\right)^{\frac{1}{2}}}=\frac{\sqrt{2}}{2}\left(1+\varepsilon^2\right)^{1/2}.$$

Then $F_\varepsilon=\mu+\sqrt{\mu}G_\varepsilon$ where

$$G_\varepsilon(v)=-\sqrt{\mu(v)}+\frac{2^{\frac{3}{4}}\left(1+\varepsilon^2\right)^{3/2}}{16\pi^{3/4}}\left(e^{-\frac{\varepsilon^2v^2}{4}}+\frac{1}{\varepsilon^3}e^{-\frac{v^2}{4\varepsilon^2}}\right)$$

or

$$G_\varepsilon(v)=-\sqrt{\mu(v)}+\frac{2^{\frac{1}{2}}\left(1+\varepsilon^2\right)^{3/2}}{8}\left(\sqrt{\mu(\varepsilon v)}+\frac{1}{\varepsilon^3}\sqrt{\mu(v/\varepsilon)}\right)$$

then $G_\varepsilon\in\mathcal{N}^\perp$. We compute from Lemma D.1

$$G_{\varepsilon,n}=(G_\varepsilon,\varphi_n)_{L^2}=I_1+\frac{2^{\frac{1}{2}}\left(1+\varepsilon^2\right)^{3/2}}{8}(I_2+I_3)$$

where

$$I_1 = (-\sqrt{\mu}, \varphi_n)_{L^2} = (-\varphi_0, \varphi_n)_{L^2} = -\delta_{0,n},$$
$$I_2 = \left(\sqrt{\mu(\varepsilon\cdot)}, \varphi_n\right)_{L^2} = (2^{\frac{9}{4}}\pi^{\frac{3}{4}})\varphi_n(0)\frac{\left(1-\varepsilon^2\right)^n}{\left(1+\varepsilon^2\right)^{n+3/2}},$$
$$I_3 = (-1)^n I_2.$$

Finally we get

$$G_{\varepsilon,n} = -\delta_{0,n} + \frac{1+(-1)^n}{2}\frac{\left(1-\varepsilon^2\right)^n}{\left(1+\varepsilon^2\right)^n}\left(\frac{(2n+1)!}{2^{2n}(n!)^2}\right)^{\frac{1}{2}}.$$

+ □

**Appendix D. Some results on the spherical harmonics.** We recall that

$$\varphi_n(v) = \left(\frac{n!}{\sqrt{2}\Gamma(n+3/2)}\right)^{1/2} e^{-\frac{|v|^2}{4}} L_n^{[\frac{1}{2}]}\left(\frac{|v|^2}{2}\right)\frac{1}{\sqrt{4\pi}}$$

where the Laguerre polynomial $L_n^{[\alpha]}$ of order $\alpha$, degree $n$ is

$$L_n^{[\alpha]}(x) = \sum_{r=0}^{n}(-1)^{n-r}\frac{\Gamma(\alpha+n+1)}{r!(n-r)!\Gamma(\alpha+n-r+1)}x^{n-r}.$$

LEMMA D.1. *For $a>0$ and $n\geq 0$ we have*

$$\varphi_n(0) = \frac{1}{(2\pi)^{\frac{3}{4}}}\left(\frac{(2n+1)!}{2^{2n}(n!)^2}\right)^{\frac{1}{2}},$$
$$\int_{\mathbb{R}^3}\varphi_n(v)dv = (-1)^n 2^3\pi^{\frac{3}{2}}\varphi_n(0),$$
$$(\sqrt{\mu(a\cdot)}, \varphi_n)_{L^2} = (2^{\frac{9}{4}}\pi^{\frac{3}{4}})\varphi_n(0)\frac{\left(1-a^2\right)^n}{\left(1+a^2\right)^{n+3/2}}.$$

*Proof.* These equalities come from classical properties of the Hermite funtions (we have checked them using Maple®13 for integers $n\leq 20$). □

**Appendix E. Maple codes.** We present the algorithms using Maple in this paper. They have been tested on version Maple13 and Maple2016.

Algorithm 1: Initialization (see (3.3) and (3.5))

```
Digits:= 20:
N:=10:

# Collision kernel: beta = 2*Pi*sin(theta)*b(cos(theta))
# beta:= (1/2)*sin(theta): theta_max:= Pi: # cutoff
s0:=1/2: beta:= 1/sin(theta/2)^(1+2*s0): theta_max:= Pi/2: # non cutoff

# Maxwellian mu1 and its square root mu2
mu1:= (2*Pi)^(-3/2)*exp(-(1/2)*v^2):
mu2:= (2*Pi)^(-3/4)*exp(-(1/4)*v^2):
```

Algorithm 2: Initial data of the BKW solution (3.4)

```
# BKW Solution
fBKW:= a1 *( (2-5*(1-K)) + (1-K)*v^2/K) * exp(-v^2/(2*K)):
a1:= (1/(2*(2*Pi)^(3/2)*K^(5/2))):
K:= 1 - exp(-t/6):

# Computation of the BKW solution at time t0 = 5.5
F_:= subs(t=5.5, fBKW):
G_:= simplify(expand( (F_ - mu1)/mu2) , exp):
```

Algorithm 3: Computation of the eigenvectors $\varphi_n(v)$ (2.3)

```
for n from 1 to N do
  a1:= sqrt(factorial(n)/(sqrt(2)*GAMMA(n+3/2))):
  f1:= exp(-(1/4)*v^2)*LaguerreL(n, 1/2, (1/2)*v^2)/sqrt(4*Pi):
  phi[n]:= simplify(a1*f1):
end do:
```

Algorithm 4: Numerical computation of the eigenvalues $\mu_{p,q}$ and $\lambda_n$ (2.6)

```
mu[0,0]:= 0: lambda[0]:= 0:
for n from 1 to N do
  # Computation of mu[0,n]
  f1:= 1 - (cos(theta/2))^(2*n):
  f2:= simplify( beta*f1 ):
  mu[0,n]:= - int(f2, theta=10^(-40)..theta_max, numeric):

  # Computation of mu[p,q], p+q=n, p>0
  for p from 1 to n do
    q:=n-p:
    a1:= ( (2*p+2*q+1)! /((2*p+1)!*(2*q+1)!) )^(1/2):
    f1:= (sin(theta/2))^(2*p) * (cos(theta/2))^(2*q):
    f2:= simplify( beta*f1 ):
    mu[p,q]:= evalf(a1) * int(f2, theta=10^(-40)..theta_max, numeric):
  end do:

  # Computation of lambda[n]
  lambda[n]:= -(mu[n,0]+mu[0,n]):
end do:
```

Algorithm 4-bis: Symbolic computation of the eigenvalues $\mu_{p,q}$ and $\lambda_n$ (2.6)

```
mu[0,0]:= 0: lambda[0]:= 0:
for n from 1 to N do
  # Computation of mu[0,n]
  f1:= 1 - (cos(theta/2))^(2*n):
  f2:= simplify( beta*f1 ):
  mu[0,n]:= - int(f2, theta=0..theta_max):

  # Computation of mu[p,q], p+q=n, p>0
```

```
  for p from 1 to n do
    q:=n-p:
    a1:= ( (2*p+2*q+1)! /((2*p+1)!*(2*q+1)!) )^(1/2):
    f1:= (sin(theta/2))^(2*p) * (cos(theta/2))^(2*q):
    f2:= simplify( beta*f1 ):
    mu[p,q]:= a1 * int(f2, theta=0..theta_max):
   end do:

  # Computation of lambda[n]
  lambda[n]:= -(mu[n,0]+mu[0,n]):
end do:
```

Algorithm 5: Computation of the spectral initial data $G_n = (G, \varphi_n)_{L^2(\mathbb{R}^3)}$

```
G[0]:=0: G[1]:=0:
for n from 2 to N do
  G[n]:= int(G_*phi[n]*4*Pi*v^2, v=0..infinity, numeric):
end do:
```

Algorithm 6: Computation of the nonlinear part $h_n(t)$ (2.8)

```
h[0]:= 0: h[1]:= 0: h[2]:= 0: h[3]:= 0:
for n from 4 to N do
  h[n]:= 0:
  for p from 2 to n-2 do
    q:=n-p:
    a1:= mu[p,q] * exp((lambda[n]-lambda[p]-lambda[q])*t):
    f1:= a1 * (G[p]+h[p]) * (G[q]+h[q]);
    f2:= subs(t = s, f1):
    f3:= int(f2, s = 0..t):
    h[n]:= h[n] + f3:
  end do:
end do:
```

Algorithm 7: Computation of the successive approximate solutions (3.1) and (3.6): $g_n^{\text{approx}}(t,v) = \sum_{k=2}^{n} e^{-\lambda_k t}(G_k + h_k(t))\varphi_k(v)$, $\quad f_n(t,v) = \mu(v) + \sqrt{\mu(v)}\, g_n^{\text{approx}}(t,v)$

```
gapprox[0]:= 0:
fapprox[0]:= mu1 + mu2 * gapprox[0]:
for n from 1 to N do
  gapprox[n]:= gapprox[n-1] +  exp(-lambda[n]*t)*(G[n]+h[n])*phi[n]:
  fapprox[n]:= mu1 + mu2 * gapprox[n]:
end do:
```

Algorithm 7-bis: Computation of the successive approximate solutions (3.1) and (3.6):
$g_n^{lin}(t,v) = \sum_{k=2}^{n} e^{-\lambda_k t} G_k \varphi_k(v)$, $\quad g_n^{n\ell}(t,v) = \sum_{k=2}^{n} e^{-\lambda_k t} h_k(t)\varphi_k(v)$,
$f_n(t,v) = \mu(v) + \sqrt{\mu(v)}\,(g_n^{lin}(t,v) + g_n^{n\ell}(t,v))$

```
glin[0]:= 0:  gnl[0]:= 0:
fapprox[0]:= mu1 + mu2 * (glin[0] +  gnl[0]):
for n from 1 to N do
  glin[n]:= glin[n-1] +  exp(-lambda[n]*t)*G[n]*phi[n]:
  gnl[n]:=  gnl[n-1] +  exp(-lambda[n]*t)*h[n]*phi[n]:
  fapprox[n]:= mu1 + mu2 * (glin[n] + gnl[n]):
end do:
```

Algorithm 8: Computation of the error between spectral and BKW solution at time T = t0 or T = t1.

```
fBKW_T:= subs(t=T, fBKW):
m1:= 0:
for v1 from -4 to 4 by 0.1 do
  a1:= evalf(subs(v=v1, fBKW_T):
  m1:= max(m1,a1):
end do:
fBKW_max:= m1:

f_T:= subs(t=T, fapprox[n]):
for n from 4 to N do
  m1:= 0:
  for v1 from -4 to 4 by 0.1 do
    a1:= evalf(subs(v=v1, abs(f_T - fBKW_T)):
    m1:= max(m1,a1):
  end do:
  erreur[n]:= m1/fBKW_max:
end do:
```

## REFERENCES


[1] R. Alexandre, Y. Morimoto, S. Ukai, C.-J. Xu, and T. Yang, *Regularizing effect and local existence for the non Cutoff Boltzmann equation*, Arch. Rational Mech. Anal., 198:39–123, 2010. 1.2

[2] M. Bennoune, M. Lemou, and L. Mieussens, *Uniformly stable numerical schemes for the Boltzmann equation preserving the compressible Navier-Stokes asymptotics*, J. Comp. Phys., 227:3781–3803, 2008. 1.2

[3] G. A. Bird, *Molecular Gas Dynamics and the Direct Simulation of Gas Flows*, Oxford University Press, Second Edition, 1994. 1.2

[4] A. Bobylev, *Exact solutions of the Boltzmann equation*, in Akademiia Nauk SSSR Doklady, 225:1296–1299, 1975. 1.2, 3, A.1

[5] A. Bobylev, *The theory of the nonlinear spatially uniform Boltzmann equation for Maxwell molecules*, Soviet Sci. Rev. Sect. C: Math. Phys., 7:111–233, 1988. 2.2

[6] A. Bobylev, A. Palczewski, and J. Schneider, *On approximation of the Boltzmann equation by discrete velocity models*, Comptes rendus de l'Académie des sciences, Série 1, Mathématique, 320(5):639–644, 1995. 1.2

[7] A. Bobylev and S. Rjasanow, *Difference scheme for the Boltzmann equation based on fast Fourier transform*, Eur. J. Mech. B Fluids, 16(2), 1997. 1.2

[8] L. Boltzmann, *Weitere studien über das wärmegleichgewicht unter gas-molekülen*, Wiener Berichte, 66:275–370, 1872. 1.1

[9] C. Buet, S. Cordier, and P. Degond, *Regularized Boltzmann operators, simulation methods in kinetic theory*, Comput. Math. Appl., 35:55–74, 1998. 1.2

[10] Z. Cai, Y. Fan, and L. Ying, *Entropy monotonic spectral method for Boltzmann equation*, arXiv:1704.07369v1 [math.NA] 2017. 1.2

[11] C. Cercignani, *The Boltzmann Equation and its Applications*, Appl. Math. Sci., Springer-Verlag, New York, 67, 1988. 1.1, 1.2, 2.1, 2.2

[12] L. Desvillettes, *Regularization properties of the 2-dimensional non radially symmetric non cut-off spatially homogeneous Boltzmann equation for Maxwellian molecules*, Tran. Theo. Stat. Phys., 26(3):341–357, 1997. 1.1, 1.2

[13] L. Desvillettes, *Regularization for the non cutoff 2D radially symmetric Boltzmann equation with a velocity dependant cross section*, Tran. Theo. and Stat. Phys., (special issue), 25(3-5):383–394, 1996. 1.1, 1.2

[14] L. Desvillettes and F. Golse, *On the smoothing properties of a model Boltzmann equation without Grad's cutoff assumption*, Proceedings of the 21st International Symposium on Rarefied Gas Dynamics, R. Brun, R. Campargue, R. Gatignol et J.-C. Lengrand éditeurs, Cépaduès éditions, Toulouse, 1:47–54, 1999. 1.1

[15] L. Desvillettes and F. Golse, *On a model Boltzmann equation without angular cutoff*, Differential and Integral Equations, 13(4-6):567–594, 2000. 1.1

[16] L. Desvillettes, *About the use of the Fourier transform for the Boltzmann equation*, Riv. Mat. Univ. Parma, 7(2):1–99, 2003. A

[17] L. Desvillettes and B. Wennberg, *Smoothness of the solution of the spatially homogeneous Boltzmann equation without cutoff*, Comm. Part. Diff. Eqs., 29(1-2):133–155, 2004. 1.1

[18] G. Dimarco and L. Pareschi, *High order asymptotic-preserving schemes for the Boltzmann equation*, C.R. Math. Acad. Sci. Paris, 350(9-10):481–486, 2012. 1.2

[19] G. Dimarco and L. Pareschi, *Asymptotic preserving implicit-explicit Runge-Kutta methods for nonlinear kinetic equations*, SIAM J. Numer. Anal., 51(2):1064–1087, 2013. 1.2

[20] G. Dimarco and L. Pareschi, *Numerical methods for kinetic equations*, Acta Numerica, Cambridge University Press (CUP), 23:369–520, 2014. 1.1, 1.2

[21] E. Dolera, *On the spectrum of the linearized Boltzmann collision operator for Maxwellian molecules*, Boll. UMI, 46:67–105, 2010. 2.2

[22] F. Filbet, C. Mouhot, L. Pareschi, *Solving the Boltzmann equation in $N\log_2 N$*, SIAM J. Sci. Comput., 28(3):1029–1053, 2007. 1.2

[23] I. M. Gamba, J. R. Haack, C. D.Hauck, and J. Hu, *A fast spectral method for the Boltzmann collision operator with general collision kernels*, SIAM J. Sci. Comput., 39(4)B658CB674, 2017. 1.2, 4.1, 4.1

[24] L. Glangetas, H.-G. Li, and C.-J. Xu, *Sharp regularity properties for the non-cutoff spatially homogeneous Boltzmann equation*, Kinet. Relat. Models, 9(2):299–371, 2016. 4.1

[25] D. Goldstein, B. Sturtevant, and J. E. Broadwell, *Investigations of the motion of discrete-velocity gases*, Progress in Astronautics and Aeronautics, 117:100–117, 1989. 1.2

[26] P.-T. Gressman and R.-M. Strain, *Global classical solutions of the Boltzmann equation without angular cut-off*, J. Amer. Math. Soc., 24(3):771–847, 2011. 1.1, 1.2

[27] S. Jin, *Runge-Kutta methods for hyperbolic conservation laws with stiff relaxation terms*, J. Comp. Phys., 122:51–67 , 1995. 1.2

[28] S. Jin, *Efficient asymptotic-preserving (ap) schemes for some multiscale kinetic equations*, SIAM J. Sci. Comput., 21(84):441–454, 1999. 1.2

[29] S. Jin, *Asymptotic preserving (AP) schemes for multiscale kinetic and hyperbolic equations: a review*, Riv. Math. Univ. Parma (N.S.), 3(2):177–216, 2012. 1.2

[30] M. Krook and T. T. Wu, *Exact solutions of the Boltzmann equation*, Phys. Fluids, 20(10):1589–1595, 1977. 1.2, 3, A.1, A.1

[31] N. Lerner, Y. Morimoto, K. Pravda-Starov, and C.-J. Xu, *Phase space analysis and functional calculus for the linearized Landau and Boltzmann operators*, Kinet. Relat. Models, 6:625–648, 2013. 2.1, 2.2

[32] N. Lerner, Y. Morimoto, K. Pravda-Starov, and C.-J. Xu, *Spectral and phase space analysis of the linearized non-cutoff Kac collision operator*, J. Math. Pures Appl., 100:832–867, 2013. 1.1, 2.1, 2.2, 3.3, A

[33] N. Lerner, Y. Morimoto, K. Pravda-Starov, and C.-J. Xu, *Gelfand-Shilov smoothing properties of the radially symmetric spatially homogeneous Boltzmann equation without angular cutoff*, J. Diff. Eqs., 256:797–831, 2014. 1.1, 2.1, 2.2, 2.2, 2.2, 3.1

[34] C. Mouhot and L. Pareschi, *Fast algorithms for computing the Boltzmann collision operator*, Math. Comp., 75(256):1833–1852, 2006. 1.2

[35] V. A. Panferov and A. G. Heintz, *A new consistent discrete-velocity model for the Boltzmann equation*, Math. Meth. Appl. Sci., 25(7):571–593, 2002. 1.2

[36] L. Pareschi and B. Perthame, *A Fourier spectral method for homogeneous Boltzmann equations*, Trans. Theo. Stat. Phys., 25(3-5):369–382, 1996. 1.2

[37] L. Pareschi and G. Russo, *Numerical solution of the Boltzmann equation I: Spectrally accurate approximation of the collision operator*, SIAM J. Numer. Anal., 37(4):1217–1245, 2000. 1.2

[38] F. Rogier and J. Schneider, *A direct method for solving the Boltzmann equation*, Trans. Theo. Stat. Phys., 23(1-3):313–338, 1994. 1.2

[39] C. Villani, *On a new class of weak solutions to the spatially homogeneous Boltzmann and Landau equations*, Arch. Rational Mech. Anal., 143:273–307, 1998. 1.2

[40] C. Villani, *A review of mathematical topics in collisional kinetic theory*, Handbook of Mathematical Fluid Dynamics, 1:71–74, 2002. 1.1